

FILM FORMATION AND CO₂ CORROSION IN THE PRESENCE OF ACETIC ACID

A thesis presented to the faculty of the
Fritz. J. and Dolores H. Russ College of Engineering and Technology of
Ohio University

In partial fulfillment
of the requirements for the degree
Master of Science

Omkar A. Nafday

August 2004

This thesis entitled
FILM FORMATION AND CO₂ CORROSION IN THE PRESENCE OF ACETIC ACID

by
Omkar A. Nafday

has been approved for the
Department of Chemical Engineering
and the Russ College of Engineering and Technology by

Srdjan Nesic
Professor of Chemical Engineering

R.Dennis Irwin
Dean, Russ College of Engineering and Technology

NAFDAY, OMKAR A. M.S. August 2004. Chemical Engineering

Film Formation and CO₂ Corrosion in the Presence of Acetic Acid (pp. 97)

Director of Thesis: Srdjan Nesic

The role of acetic acid (HAc) on the protectiveness of iron carbonate (FeCO₃) films in CO₂ corrosion has been investigated using electrochemical, scanning electron microscopy (SEM) and x-ray diffraction (XRD) techniques. HAc has recently been recognized as a major factor in premature pipeline failure causing either generalized or localized corrosion. The main cause of concern is the undissociated (free) HAc which is found in oilfield brines. The pH value of the brine determines both the amount of free HAc and the supersaturation (SS). In order for a protective FeCO₃ film to form, the SS value is critical. A series of experiments was performed to test the effect of various amounts of free HAc on cylindrical X-65 steel coupons at different values of pH at stagnant (no rotation) conditions. A 3% sodium chloride (NaCl) salt solution by weight was used to simulate oilfield brine. All experiments were conducted at fixed pH, 80°C to accelerate film formation. In order to ascertain that a FeCO₃ film was indeed formed, a XRD scan was conducted on the film observed on the sample at the end of experiment and the matching of constituent element peaks confirmed a FeCO₃ film.

HAc was found to have no effect on film formation and on the final corrosion rates of X-65 mild steel. The SEM pictures show no effect of HAc on film formation and protectiveness at a fixed pH. No evidence of localised corrosion (pitting) was observed on the specimens.

Approved: Srdjan Nesic

Professor of Chemical Engineering

Dedication

To

Anand and Madhavi Nafday (my Parents)

and

Ojas Nafday (brother)

for their encouragement and guidance throughout my life.

Without their sacrifice and support, I would not have been able to reach for new horizons.

Acknowledgements

The author would like to thank his advisor, Dr. Srdjan Nestic, for the advice and support he gave not only during the experimental program but also during the entire thesis work. It was an honor to work under his supervision.

Dr. Daniel Gulino and Dr. Howard Dewald have also contributed significantly with their advice and mentoring throughout this project.

The author would also like to thank Bruce Brown, Al Schubert and John Goettge, the technical staff at the Institute for Corrosion and Multiphase technology for their help in experimental issues.

The author thanks fellow co-workers and students (Kunal Chokshi, Wei Sun, Marc Singer, Conchita Mendez and Peter Okafor) for their advice and opinions throughout this project.

Last but not least the author acknowledges the financial and technical support of the Consortium (BP, Shell, Exxon Mobil, Saudi Aramco, Total, Clariant, Petrobras, Agip, Nalco, Champion, MI Chemicals) of member companies who have given this project direction whenever needed.

Table of Contents

Abstract.....	3
Dedication.....	4
Acknowledgements.....	5
Table of Contents.....	6
List of Tables.....	8
List of Figures.....	9
1. Introduction.....	14
2. Literature Review.....	17
2.1 CO ₂ corrosion.....	17
2.2 Acetic Acid Corrosion.....	18
2.3 Iron carbonate (FeCO ₃) film formation.....	21
2.4 Mechanical Integrity of iron carbonate (FeCO ₃) film.....	23
3. Test Matrix and Research Objectives.....	25
4. Experimental Setup and Procedure.....	28
4.1 Electrochemical measurements.....	30
4.2 X-65 mild steel working electrode.....	30
4.3 Post-experimental analysis.....	31
5. Results.....	32
5.1 Baseline tests at pH 6.6, stagnant conditions.....	33
5.2 Supersaturation (SS) of 162.....	35

5.2.1 Film integrity experiments at supersaturation (SS) of 162.....	48
5.3 Supersaturation (SS) of 41.....	53
5.4 Supersaturation (SS) of 32.....	56
5.5 Supersaturation (SS) of 10.....	66
5.6 Discussion.....	70
5.7 Comparison with MULTICORP Version 3.0.....	72
6. Conclusion.....	77
7. References.....	78
APPENDIX A: METHOD OF Fe ²⁺ ADDITION	81
APPENDIX B: TAFEL SLOPES	83
APPENDIX C: CORROSION RATE MEASUREMENT	85
APPENDIX D: EXPERIMENTAL UNCERTAINTY ANALYSIS	86
APPENDIX E: SUPERSATURATION CALCULATION	95
APPENDIX F: METHOD OF SAMPLE CLEANING	96

List of Tables

Table 1.1: HAc identification and physical and chemical properties	16
Table 3.1: Test matrix for the research	25
Table 4.1: Chemical composition of X-65 steel (wt %)	31
Table 5.1: HAc dissociation at fixed pH value	33
Table 5.2: HAc dissociation at different pH values	33

List of Figures

Figure 4.1: Schematic of the glass cell.	29
Figure 4.2: Sample encased halfway in epoxy.....	31
Figure 5.1: Average corrosion rate variation with time in experiments without HAc at pH 6.6, 80°C, 10 and 50 ppm Fe ²⁺ , at stagnant pure film formation conditions. (Error bars represent the maximum and minimum values of corrosion rate observed).....	34
Figure 5.2: Average corrosion rate plot with time in experiments without and with 18 ppm free HAc (1000 ppm total) at SS = 162, pH 6.6, 80°C, 50 ppm Fe ²⁺ . (Error bars represent the maximum and minimum values of corrosion rate observed, refer to Figure 5.3 for the curves in the logarithmic scale, 5.4 for SEM front view and 5.5 for SEM cross-sectional view.).....	36
Figure 5.3: Corrosion rate progression with time in the logarithmic scale at SS = 162, pH 6.6, T = 80°C, 50 ppm Fe ²⁺ , without and with 18 ppm free HAc, stagnant conditions. (Refer to Figure 5.2 for the average curves, 5.4 for SEM front view and 5.5 for SEM cross-sectional view.).....	37
Figure 5.4: Front view pictures of FeCO ₃ film at SS = 162, pH 6.6, 80°C, 50 ppm Fe ²⁺ , without and with 18 ppm free HAc, stagnant condition. (Refer to Figure 5.2 for the average curves, 5.3 for all the curves on the logarithmic scale, 5.5 for SEM cross-sectional view.).....	38
Figure 5.5: SEM pictures (cross sectional view) of FeCO ₃ film at 500X, SS = 162, pH 6.6, 80° C, 50 ppm Fe ²⁺ , 18 ppm free HAc, stagnant condition. (Refer to Figure 5.2 for the average curves, 5.3 for all the curves on the logarithmic scale, 5.4 for SEM front view)	39
Figure 5.6: Average corrosion rate plot with time in experiments without and with 72 ppm free HAc (4000 ppm HAc total) at SS = 162, pH 6.6, 80° C, 50 ppm Fe ²⁺ (Error bars represent the maximum and minimum values of corrosion rate observed, refer to Figure 5.7 for the curves in the logarithmic scale, 5.8 for SEM front view and 5.9 for SEM cross-sectional view.).....	40
Figure 5.7: Corrosion rate progression with time in the logarithmic scale at SS = 162, pH 6.6, T = 80°C, 50 ppm Fe ²⁺ , without and with 72 ppm free HAc, stagnant conditions. (Refer to Figure 5.6 for the average curves, 5.8 for the front view and 5.9 for SEM cross-sectional view)	41
Figure 5.8: Front view pictures of FeCO ₃ film at SS = 162, pH 6.6, 80°C, 50 ppm Fe ²⁺ , without and with 72 ppm free HAc, stagnant condition. (Refer to Figure 5.6 for the average curves, 5.7 for the curves in the logarithmic scale, 5.9 for the cross-sectional view)	42

Figure 5.9: SEM pictures (cross sectional view) of FeCO_3 film at 500 X, SS = 162, pH 6.6, 80°C, 50 ppm Fe^{2+} , with 72 ppm free HAc, stagnant condition. (Refer to Figure 5.6 for the average curves, 5.7 for the curves in the logarithmic scale, 5.8 for the front view.)	43
Figure 5.10: Average corrosion rate plot with time in experiments without and with 180 ppm free HAc (10,000 ppm HAc total) at SS = 162, pH 6.6, 80°C, 50 ppm Fe^{2+} (Error bars represent the maximum and minimum values of corrosion rate observed, refer to Figure 5.11 for the curves in the logarithmic scale, 5.12 for SEM front view and 5.13 for SEM cross-sectional view.)	44
Figure 5.11: Corrosion rate progression with time in the logarithmic scale at pH 6.6, T = 80°C, 50 ppm Fe^{2+} , without and with 180 ppm free HAc, stagnant conditions. (Refer to Figure 5.10 for the average curves, 5.12 for SEM front view and 5.13 for SEM cross-sectional view)	45
Figure 5.12: Front view pictures of FeCO_3 film at SS = 162, pH 6.6, 80°C, 50 ppm Fe^{2+} , without and with 180 ppm free HAc, stagnant condition. (Refer to Figure 5.10 for the average curves, 5.11 for the curves in the logarithmic scale, 5.13 for SEM cross-sectional view)	46
Figure 5.13: SEM pictures (cross sectional view) of FeCO_3 film at 500 X, SS = 162, pH 6.6, 80°C, 50 ppm Fe^{2+} , 180 ppm free HAc, stagnant condition. (Refer to Figure 5.10 for the average curves, 5.11 for the curves in the logarithmic scale, 5.12 for the front view)	47
Figure 5.14: Comparison of the average curves at SS = 162, pH 6.6, 80°C, 50 ppm Fe^{2+} , with 18, 72 and 180 ppm free HAc, stagnant condition. (Error bars represent the maximum and minimum values of corrosion rates observed)	48
Figure 5.15: Corrosion rate variation with time in rotation experiments at SS = 162, 0 and 9000 rpm without HAc at pH 6.6, 80°C, 50 ppm Fe^{2+} . (Refer to Figure 5.16 for curves in the logarithmic scale)	49
Figure 5.16: Corrosion rate progression with time in the logarithmic scale at SS = 162, pH 6.6, T = 80°C, 50 ppm Fe^{2+} , without HAc, stagnant and 9000 rpm conditions. (Refer to Figure 5.15 for curves in the normal scale)	50
Figure 5.17: Corrosion rate variation with time in rotation experiments at SS= 162, 0 and 9000 rpm with 72ppm free HAc at pH 6.6, 80°C, 50 ppm Fe^{2+} . (Refer to Figure 5.18 for curves in the logarithmic scale)	51
Figure 5.18: Corrosion rate progression with time in the logarithmic scale at SS = 162, pH 6.6, T = 80°C, 50 ppm Fe^{2+} , with 72 ppm free HAc, stagnant and 9000 rpm conditions. (Refer to Figure 5.17 for curves in the normal scale)	51

- Figure 5.19: SEM pictures (frontal view) of FeCO_3 film at SS = 162, pH 6.6, 80°C, 50 ppm Fe^{2+} , 0 and 9000 rpm condition at 1500 X. (Refer to Figure 5.20 for SEM cross-section pictures.) 52
- Figure 5.20: SEM pictures (cross sectional view) of FeCO_3 film at 500 X, SS = 162, pH 6.6, 80°C, 50 ppm Fe^{2+} , 0 and 9000 rpm. (Refer to Figure 5.19 for SEM front view pictures.)..... 52
- Figure 5.21: Average corrosion rate with time in experiments with and without 35 ppm free HAc (1000 ppm HAc total) at SS = 41, pH 6.3, 80°C, 50 ppm Fe^{2+} (Error bars represent the maximum and minimum values of corrosion rate observed, refer to Figure 5.22 for the curves in the logarithmic scale, 5.23 for SEM front view and 5.24 for SEM cross-sectional view.)..... 54
- Figure 5.22: Corrosion rate progression with time in the logarithmic scale at SS = 41, pH 6.3, T = 80°C, 50 ppm Fe^{2+} , without and with 35 ppm free HAc, stagnant conditions. (Refer to Figure 5.21 for the average curves, 5.23 for SEM front view and 5.24 for SEM cross-sectional view.)..... 55
- Figure 5.23: SEM pictures (frontal view) at 1500 X of FeCO_3 film at SS = 41, pH 6.3, 80°C, 50 ppm Fe^{2+} , stagnant condition. (Refer to Figure 5.21 for the average curves, 5.22 for the curves in the logarithmic scale, 5.24 for SEM cross-sectional view.) 55
- Figure 5.24: SEM pictures (cross sectional view) of FeCO_3 film at 500 X, pH 6.3, 80°C, 50 ppm Fe^{2+} , stagnant condition. (Refer to Figure 5.21 for the average curves, 5.22 for the curves in the logarithmic scale, 5.23 for SEM front view.) 56
- Figure 5.25: Average corrosion rate variation with time in experiments without and with 72 ppm free HAc (4000 ppm HAc total) at SS = 32, pH 6.6, 80°C, 10 ppm Fe^{2+} . (Error bars represent the maximum and minimum values of corrosion rate observed, refer to Figure 5.26 for the curves in the logarithmic scale, 5.27 for SEM front view and 5.28 for SEM cross-sectional view.) 57
- Figure 5.26: Corrosion rate progression with time in the logarithmic scale at SS = 32, pH 6.6, T = 80°C, 10 ppm Fe^{2+} , without and with 72 ppm free HAc, stagnant conditions. (Refer to Figure 5.25 for the average curves, 5.27 for SEM front view and 5.28 for SEM cross-sectional view.)..... 58
- Figure 5.27: Front view pictures of FeCO_3 film at SS = 32, pH 6.6, 80°C, 10 ppm Fe^{2+} , without and with 72 ppm free HAc, stagnant condition. (Refer to Figure 5.25 for the average curves, 5.26 for curves in the logarithmic scale, 5.28 for SEM cross-sectional view.) 59
- Figure 5.28: SEM pictures (cross sectional view) of FeCO_3 film at 500 X, SS = 32, pH 6.6, 80°C, 10 ppm Fe^{2+} , 72 ppm free HAc, stagnant condition. Refer to Figure 5.25 for the average curves, 5.26 for curves in the logarithmic scale, 5.27 for SEM front view.) 60

- Figure 5.29: Average corrosion rate variation with time in experiments without and with 180 ppm free HAc (10000 ppm HAc total) at SS= 32, pH 6.6, 80°C, 10 ppm Fe²⁺ (Error bars represent the maximum and minimum values of corrosion rate observed, refer to Figure 5.30 for the curves in the logarithmic scale, 5.31 for SEM front view and 5.32 for SEM cross-sectional view.) 62
- Figure 5.30: Corrosion rate progression with time in the logarithmic scale at SS = 32, pH 6.6, T = 80°C, 10 ppm Fe²⁺, without and with 180 ppm free HAc, stagnant conditions. (Refer to Figure 5.29 for the average curves, 5.31 for SEM front view and 5.32 for SEM cross-sectional view.)..... 63
- Figure 5.31: Front view pictures of FeCO₃ film at SS = 32, pH 6.6, 80°C, 10 ppm Fe²⁺, without and with 180 ppm free HAc, stagnant condition. (Refer to Figure 5.29 for the average curves, 5.30 for the curves in the logarithmic scale, 5.32 for SEM cross-sectional view) 64
- Figure 5.32: SEM pictures (cross sectional view) of FeCO₃ film at 500 X, SS = 32, pH 6.6, 80°C, 10 ppm Fe²⁺, 180 ppm free HAc, stagnant condition. (Refer to Figure 5.29 for the average curves, 5.30 for the curves in the logarithmic scale, 5.31 for SEM front view) 65
- Figure 5.33: Comparison of the average curves at SS = 32, pH 6.6, 80°C, 10 ppm Fe²⁺, with 72 and 180 ppm free HAc, stagnant condition in the logarithmic scale.(Error bars represent maximum and minimum values of corrosion rates)..... 66
- Figure 5.34: Average corrosion rate with time in experiments with and without 68 ppm free HAc (1000 ppm HAc total) at SS = 10, pH 6, 80°C, 50 ppm Fe²⁺(Error bars represent the maximum and minimum values of corrosion rate observed, refer to Figure 5.35 for the curves in the logarithmic scale) 67
- Figure 5.35: Corrosion rate progression with time in the logarithmic scale at SS = 10, pH 6, T = 80°C, 50 ppm Fe²⁺, without and with 68 ppm free HAc, stagnant conditions. (Refer to Figure 5.34 for the average curves.) 68
- Figure 5.36: XRD Spectrum of protective film showing it to be iron carbonate.....69
- Figure 5.37: Comparison of experimental results with OU model at SS = 162, pH = 6.60, 80°C, 50 ppm Fe²⁺, without and with 18 ppm free HAc, stagnant conditions. (Data points indicate experimental results and lines indicate OU model, refer to Figure 5.38 for the comparison of film thicknesses.) 74
- Figure 5.38: Predicted and experimentally measured iron carbonate scale thickness, at SS = 162, pH = 6.60, 80°C, 50 ppm Fe²⁺ with 18 ppm free HAc, stagnant conditions. (Refer to Figure 5.37 for the corrosion rate comparison.) 75
- Figure 5.39: Comparison of experimental results with OU model at SS = 32, pH = 6.60, 80°C, 10 ppm Fe²⁺ without and with 180 ppm free HAc, stagnant conditions. (Data points

indicate experimental results and lines indicate OU model, refer to Figure 5.40 for the comparison of film thicknesses.)	75
Figure 5.40: Predicted and experimentally measured iron carbonate scale thickness, at SS = 32, pH = 6.60, 80°C, 10 ppm Fe ²⁺ with 180 ppm free HAc, stagnant conditions. (Refer to Figure 5.39 for the corrosion rate comparison.)	76
Figure D.1: A typical linear polarization curve obtained in experiments before film formation.....	89
Figure D.2: A typical linear polarization curve obtained in experiments after film formation.....	90
Figure D.3: Comparison of the calculated and the experimental error at supersaturation of 162 and T = 80°C.....	94
Figure D.4: Comparison of the calculated and the experimental error at supersaturation of 32 and T = 80°C.....	94

1. Introduction

CO₂ corrosion in the presence of acetic acid (HAc) is recognized as a major cause of premature failure of mild steel pipelines in the oil and gas industry. CO₂ is present as a dissolved gas in the water/brine that accompanies oil production at high pressures common in underground oil and gas reservoirs. In the dissolved state it forms carbonic acid. The brine is largely a NaCl solution, but it also contains other metal ions such as Na⁺, K⁺, Ca²⁺, Mg²⁺, Cl⁻, SO₄²⁻ and organic acids the most common of which is HAc. Premature failure results in millions of dollars in property damage worldwide besides lost production and bodily injury. It is caused by the presence of a complex variety of flow regimes, multiphase flow conditions and the presence of organic acids the most common of which is HAc. The material of construction for pipelines in the oil and gas industry is carbon steel for the majority of facilities in production installations, because of its economical price, strength and easy availability. However carbon steel has a tendency to corrode in the presence of CO₂ and organic acids such as acetic acid. It is therefore important to investigate the conditions in which HAc causes corrosion damage.

Acetic acid (HAc) is the most common of organic acids found in oilfield brines. Table 1.1 shows the relevant product identification information and typical physical and chemical properties of pure HAc. It is known that the water chemistry of the brine can influence the corrosion of a metal either through the thermodynamics and kinetics of the reactions involved or by affecting protective film formation. Preliminary laboratory studies conducted as early as 1950, involving short exposures of polished steel specimens revealed no difference between CO₂ corrosion without and with HAc. Thus for a long

time, the effect of organic acids in CO₂ corrosion was largely forgotten. Since then numerous studies have been conducted both in the laboratory and the field to demonstrate that acetic acid indeed acts as a source of H⁺ ions leading to higher corrosion than that obtained in pure CO₂ environments. It was determined that the main cause of concern was the undissociated (free) HAc present at a certain pH and not the total concentration of HAc. Therefore in this study, the HAc concentrations are reported in terms of the free amounts present at a certain pH.

In CO₂ corrosion, iron carbonate (FeCO₃) film is the chief corrosion product formed and is formed through the reaction between carbonic acid, source of carbonate ions, (CO₃²⁻) and iron (Fe²⁺) released through corrosion of the pipeline. FeCO₃ forms on the wall of the pipe if the product of ferrous ion concentration (Fe²⁺) and carbonate ion concentration (CO₃²⁻) exceeds the solubility product limit. The film is known to be protective and the corrosion rate drops once the film starts growing. Although iron carbonate film formation mechanisms and kinetics have been extensively studied, it is not known how protective the film will be in the presence HAc. Moreover it is not known if the film failure (if any) is a result of a lower system pH or the result of interaction between corrosion products and HAc. Thus it becomes imperative to understand how FeCO₃ precipitation is affected in the presence of HAc, as also by the pH, temperature and ionic strength of the solution.

Before venturing into the experimental findings of this study, however a brief literature review of CO₂ corrosion, the role of acetic acid and iron carbonate film formation is in order.

Table 1.1: HAc identification and physical and chemical properties⁺⁺

Synonyms	Acetic acid, ethanoic acid, methane carboxylic acid
CAS number	64-19-7
Molecular weight	60.05
Chemical formula	CH ₃ COOH
Appearance	Clear, colorless liquid
Odor	Strong vinegar-like.
Solubility	Infinitely soluble
Density (gm/cc)	1.05
pH	2.4 (1 M solution)
Boiling point	118 °C
Vapor density at 1 bar and 118°C (gm/cc)	1.87
Auto-ignition temperature	427 °C
OSHA airborne permissible exposure limit (PEL)	10 ppm.

⁺⁺ Mallinckrodt / J.T. Baker Chemicals

2. Literature Review

2.1 CO₂ corrosion

CO₂ corrosion of steel has been the subject of a wide area of research spanning decades particularly with reference to issues of corrosion and pipeline failure in the oil and gas production and transportation industry. Although the factors which influence the rate and type of corrosion have been identified, the interactions between them at various conditions are still the subject of research today. One of the earliest efforts to explain the mechanism of CO₂ corrosion was the direct reduction of carbonic acid as explained by de Waard and Milliams¹. (1975). More recently Nesic et al.^{2,3,4} (1995, 2001, 2003) have proposed models to predict CO₂ corrosion of mild steels based on their independent body of work. The following is a summary of reactions which define CO₂ corrosion.

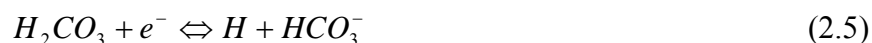
CO₂ dissolves in water to form carbonic acid through the hydration of water.



Carbonic acid dissociates to form bicarbonate which also dissociates to give carbonate and hydrogen ions.



deWaard and Milliams explained that the rate determining step for carbonic acid dissociation is the direct reduction of carbonic acid (H₂CO₃) and the corrosion rate is governed by the amount of undissociated acid in solution.





The corresponding iron dissolution reaction is



The insoluble corrosion product of reactions 2.3, 2.4 and 2.7 is iron carbonate which forms by the reaction



Another type of corrosion product is cementite (Fe_3C) which is usually formed at low temperatures in the range of 20- 40 °C as observed by Dugstad⁵ (1992). This film is the result of the iron carbide phase in the steel which survives on the surface of the metal without getting oxidized.

The corrosion rate in the presence of films depends on electrochemical reactions at the metal surface. A model to predict this was successfully proposed by Netic et al³. (2001), which took into account the reactions and transport processes.

2.2 Acetic Acid Corrosion

The influence of HAc on the rate of corrosion of mild steel in oilfield brines containing CO_2 is well documented in literature and has been the subject of numerous studies since the 1980's. Its presence was clubbed together with "organic acids" or based on the measurement of a mean molecular weight of organic acids, that of propionic acid. In the case of carbon steel in brine, the dominating factor influencing the corrosion rate is the presence of acetate (Ac^-) and dissolved CO_2 gas resulting in the formation of acetic acid. In this situation, genuine acetic acid corrosion occurs, controlled by the solubility equilibrium with a gas phase containing HAc vapor, as in the case of CO_2 corrosion.

As early as 1983, Crolet and Bonis⁶ (1983) reported that the presence of acetic acid in the brine could increase the corrosion rate of carbon steel significantly. Hedges and McVeigh⁷ (1999) later confirmed this but the interconversion of HAc and Ac⁻ ions as given by Equation 2.9 was not accounted for. In the presence of Ac⁻ ions, the corrosion rate can increase even if the pH increases leading to errors in prediction models for corrosion rates. The presence of both HCO₃⁻ and Ac⁻ cause erroneous titration results leading to an overestimation of pH.

The presence of acetate (Ac⁻) is the result of which comes from the dissociation of HAc



leads to an overestimation of pH when the HCO₃⁻ analysis is carried out leading to significant under prediction of corrosion rates. The equilibrium constant for equation 2.9 is K_{HAc} and expressed as

$$K_{HAc} = \frac{[H^+][Ac^-]}{[HAc]} \quad (2.10)$$

K_{HAc} is dependent on temperature (T_c , Celsius) and was first expressed by Kharaka et al.⁸(1989)

$$K_{HAc} = 10^{-(6.66104 - 0.0134916*(273+T_c) + 2.37856*10^{-5}*(273+T_c)^2)} \quad (2.11)$$

In equation 2.10 the total amount of HAc, $[HAc]$ and the temperature are known so K_{HAc} is also known. Thus the concentration of H⁺ ions, $[H^+]$ or the pH value determines how much of the acetic acid will dissociate. Thus different pH values represent different amounts of undissociated (free) HAc which is the main cause of

concern as it was found to increase the corrosion rate. HAc acts as a reservoir of H^+ ions, which readily accept electrons produced by the iron dissolution reaction. This drives the anodic iron dissolution reaction forward and leads to even more corrosion. George⁹ (2003) suggested that HAc does not affect the charge transfer mechanism of the cathodic reaction but only affects the limiting currents. The corrosion rate of X-65 carbon steel in the presence of HAc is under charge transfer control and both the anodic and cathodic reactions remained the same. Acetic acid was found to increase X-65 carbon steel corrosion rates greatly at pH 4 as found by this author in a separate series of experiments not included in this project.

Sidorin¹⁰ (2003) did voltammetry experiments on steel rotating disc electrode (RDE) and found that solutions containing Ca^{2+} and Fe^{2+} ions do not change the equilibrium concentration of HAc significantly although they increase the ionic strength of the solution.

Crolet et al.¹¹ (1999) showed that for uniform corrosion beneath a protective layer the free HAc is exhausted and in such a situation the acetic buffer was decisive in determining the protectiveness of corrosion products. He also reported an inhibition of the anodic dissolution reaction of iron in presence of Ac^- ions.

Garsany et al.^{12,13,14} (2002,2003) in their work used cyclic voltammetry to study the effect of Ac^- ions on the rates of corrosion using a rotating disc electrode (RDE) in the absence of film formation. They emphasized that the electrochemistry of acetic acid at steel cannot be distinguishable from that of free proton (because of its rapid dissociation) and predicted that the increased rate of corrosion is proportional to the concentration of undissociated acetic acid in the brine. Garsany et.al further suggested

that the rate of corrosion could be predicted if the speciation within the brine was calculated. To this effect, a program available on the Internet (PHREEQC 2.2, <http://www.hydroweb.com/groundwater-models-kit.html>) was used to calculate the speciation within the brine and to calculate the influence of acetate (Ac^-) ions, ionic strength, partial pressure of CO_2 , temperature, pH, etc. on the equilibrium concentration of acetic acid. He also hinted that the chemical reactions between the acetic acid and the corrosion film lead to film thinning and thus an increase in corrosion rates.

Joosten et al.¹⁵(2002) examined acetic acid, synthetic seawater and an oil phase in glass cells and found that HAc increased the corrosion rate by decreasing the pH. He also found evidence of localized 13% Cr steel at 95°C and 600 ppm HAc (total, free + dissociated).

George⁹ (2003) investigated the effects of HAc on the cathodic and anodic reactions of CO_2 corrosion using linear polarization resistance (LPR), electrochemical impedance spectroscopy (EIS) and potentiodynamic sweeps. He concluded that HAc did not affect the charge transfer mechanism of the cathodic reaction but did affect the limiting currents. At room temperature (22°C) the HAc acts as a source of hydrogen ions and HAc needs an “activation time” for its effect to be measured.

Thus experiments of long duration (3 days) were conducted at film forming conditions of high temperature (80°C) and high pH to see the effect of HAc on the film and the corrosion rate.

2.3 Iron carbonate (FeCO_3) film formation

Iron carbonate (FeCO_3) film formation is the main corrosion product in the CO_2 corrosion process. The reaction for formation of solid iron carbonate is given by:



FeCO₃ forms on the wall of the pipe if the product of ferrous ion concentration (Fe²⁺) and carbonate ion concentration (CO₃²⁻) exceeds the solubility product limit. A measure of when the film is likely to precipitate is the supersaturation value (SS) defined as

$$SS = \frac{[Fe^{2+}][CO_3^{2-}]}{[K_{sp_{FeCO_3}}]} \quad (2.13)$$

The film will precipitate when the SS value exceeds unity. However, the rate of precipitation of iron carbonate can be so slow that often the precipitation kinetics becomes more important than the thermodynamics of the process. The equilibrium constant for iron carbonate film $K_{sp_{FeCO_3}}$ is dependent on temperature (T_c , Celsius) and ionic strength (I) and expressed as

$$K_{sp_{FeCO_3}} = 10^{(-10.13 - 0.0182 * T_c)} / (0.0115 * I^{-0.6063}) \quad (2.14)$$

$$I = 0.5 * \sum_i nZ^2 \quad (2.15)$$

where i represents the number of ions, Z is charge of each ion and n is the molar concentration of each ion.

Johnson and Tomson¹⁶ (1991) used a “temperature ramped” approach to calculate the activation energy of FeCO₃ precipitation and found that precipitation was controlled by the surface reaction rate. The most important factors which affect the precipitation of iron carbonate film are supersaturation and temperature. The film is known to be protective and corrosion rate drops once the film starts growing. When FeCO₃ protective film forms, its growth is very temperature sensitive. Its composition, structure and thickness and

physical properties are determined by the film precipitation mechanisms. A frequently used expression for the rate of precipitation of the iron carbonate ($R_{FeCO_3(s)}$) is given by Van Hunnik et al.¹⁷(1996)

$$R_{FeCO_3(s)} = \frac{A}{V} \cdot f(T) \cdot K_{sp} \cdot f(SS) \quad (2.16)$$

where A is the surface area of the electrode and V the solution volume.

Since CO_3^{2-} ion concentration is dependent on the pH, we can write

$$SS = f(Fe^{2+}, pH) \quad (2.17)$$

When iron carbonate precipitates at the steel surface, it decreases the corrosion rate by

- Presenting a diffusion barrier for the species involved in the corrosion process
- Blocking a portion of the steel and preventing electrochemical reactions from occurring.

Studies by Ikeda¹⁸ et al. (1984) indicate three types of films: at low temperatures (<60°C) the film is not adherent and is easily destroyed, at 60° -150° C a loosely adherent $FeCO_3$ precipitate causes deep pitting and very high corrosion rates, at temperatures >150° C an adherent scale forms limiting corrosion. The film can be formed at room temperature by increasing system pH as indicated by Videm and Dugstad¹⁹ (1989). Dugstad⁵ (1992) showed that films were formed at 80°C after only 20-24 hours.

2.4 Mechanical Integrity of iron carbonate ($FeCO_3$) film

Schmitt et.al²⁰ (1999) in their paper on the physical properties of iron carbonate film have laid down the equations and values for parameters such as Young's Modulus (E), fracture stress (σ_y) and strain (ϵ_y), intrinsic stress intensity (K_{res}) and

intrinsic stress (σ_{sc}) They used the micro indentation method, the four-point loading and dilatometric tests while testing for cracking of the film using acoustic emission plotting. The major drawback of this method is that we do not know how much of the indentation/bending force is being distributed between the metal substrate and the film which is formed on it. The use of elaborate and sensitive equipment like dilatometric and micro-indentation methods is also cumbersome.

A novel method is being tested at the Institute for Corrosion and Multiphase Technology involving the use of water-soluble polymers. The idea is to increase the viscosity of the 3 % NaCl salt solution by adding polymers to a value sufficiently high so that when the metal sample is rotated at high speeds (9000 rpm) the shear stress at the metal surface will cause the film formed to disintegrate. The advantage of this method is that we get a realistic estimation of the toughness of iron carbonate film to withstand shear/erosion effects. This method does not need elaborate equipment, is in-situ and easy to operate. Rotation experiments will be conducted in the presence of a certain concentration of free acetic acid at an initial SS = 162, to determine if rotation has any detrimental effect on the corrosion rates.

3. Test Matrix and Research Objectives

The principal questions that need to be asked are:

1. How does the presence of HAc affect protective iron carbonate film formation?
2. How is the corresponding corrosion rate affected?
3. Does the interaction between HAc and iron carbonate affect the characteristics (thickness, protectiveness) of the film formed?

The following test matrix was performed to answer the above questions.

Table 3.1: Test matrix for the research

Parameter	Value
Steel type	X-65
Solution	3% NaCl
De-oxygenation gas	CO ₂
pH	6.6, 6.3, 6.0
Total HAc (ppm)	1000, 4000, 10000
Temperature (°C)	80
Fe ²⁺ (ppm)	10, 50
Rotational velocity (rpm)	0, 9000
Sand paper grit used	220, 400, 600
Measurement techniques	LPR, EIS, SEM, WL, XRD

Where LPR is linear polarization resistance, EIS is electrochemical impedance spectroscopy, SEM is scanning electron microscopy, WL is weight loss method for corrosion rate determination and XRD is X-ray diffraction. The above test matrix was chosen to reflect conditions in the field. However all the combinations possible from the test matrix were not conducted.

The temperature was fixed at 80°C in order to simulate a typical condition observed in the field and to facilitate rapid film formation. A 3% NaCl salt (by wt.) solution was used to simulate sea water/ brine. The total HAc added is specified in Table 3.1. The same total HAc amount at different pH values corresponds to different amounts of undissociated HAc. The different pH and Fe^{2+} concentrations also represent different supersaturation values. The experiments were conducted for duration of upto 80 hours in order to see the long-term effect of HAc on film formation.

4. Experimental Setup and Procedure

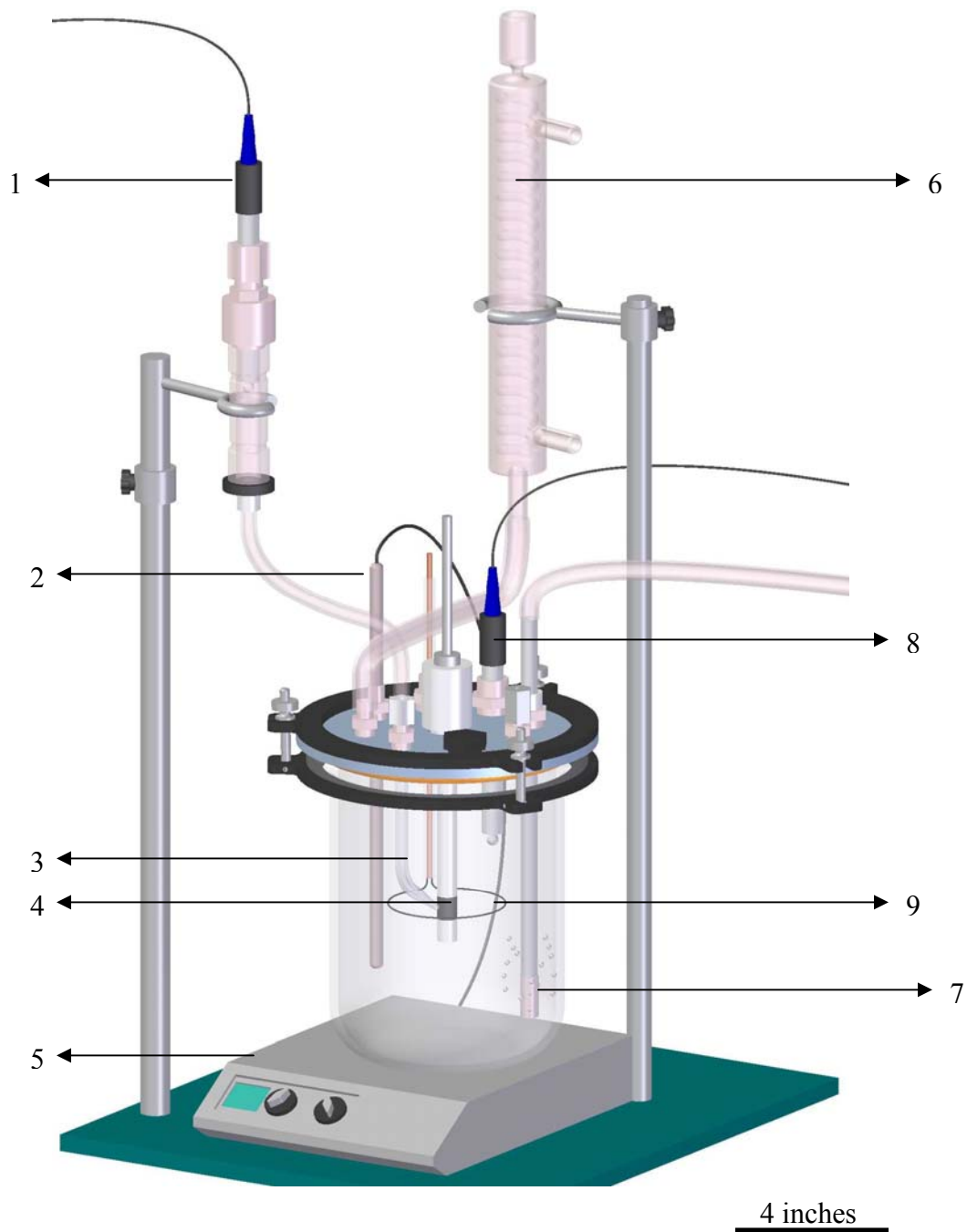
The experiments were performed in a glass cell, on a small scale in order to obtain data quickly and reproducibly. A schematic representation of the glass cell is shown in Figure 4.1.

The glass cell was filled with two liters of deionised (DI) water to which 3% by weight of NaCl salt was added. For achieving 3% NaCl concentration, 60.6 g of ACS grade, >99.7% pure NaCl was weighed and added. 1 M KCl solution used as a salt bridge between the reference and working electrode (WE, X-65 sample). The counter electrode (CE) used was a concentric platinum ring. CO₂ gas is used to deoxygenate the solution for about an hour. The temperature is set on the hot-plate and controlled with a temperature probe forming the feedback loop.

Once deoxygenation has been achieved the desired concentration of Fe²⁺ (50 or 10 ppm) was then added to the cell by dissolving FeCl₂·4H₂O crystals in DI water. This represents only the initial value of iron concentration, and as the experiment progressed the iron count steadily decreased to less than 0.5 ppm. For the purpose of preparation of iron (II) chloride containing solutions, to avoid oxidation of FeCl₂ to FeCl₃ the powder of FeCl₂ was added after degassing the solution with nitrogen or CO₂ for 30 minutes. New solution was prepared for each experiment. For example for achieving 50 ppm Fe²⁺ concentration, 1.8 gm of FeCl₂·4H₂O crystals were dissolved in 100 ml of deoxygenated DI water and then 20 ml of this solution was added to the cell. Regular monitoring of the Fe²⁺ concentration was done throughout the duration of the experiment using Turner SP-780 spectrophotometer and FerroVer (iron phenanthroline) reagent available in ready to use pouches. The pH of the solution was measured using an Oakton

glass pH meter and a Cole-Palmer AgCl pH electrode. The pH was maintained at the desired value by minute addition of hydrochloric acid (HCl) or NaHCO₃ as applicable. The specimen was polished successively using 220, 400 and 600 grit sand paper. Since FeCO₃ film precipitation is very surface sensitive, it was important to polish the metal coupon to a uniform finish in all the experiments for reproducible results.

The specimen was immersed in the test solution and the potentiostat electrical connections were made and measurements started. At the end of the test, the sample was removed from the cell and stored in a moisture free cabinet for SEM analysis of the film. The SEM unit was a JOL-JSM 5300 with a 30 kV acceleration voltage having a tungsten filament. The range of magnifications possible was 35 X – 2,00,000 X and magnified images could be captured using DSG digital imaging software. The XRD scan was conducted using a Rigakau D/B Max. unit having a copper k-alpha radiation target. The range of angles that could be obtained was 5° – 160°. On the detector side, the unit had a curved crystal monochromatometer which allowed both k-alpha and k-beta emissions. The optical microscope was an “Accu-scope” model with an eye-piece of 10 X and having the lenses capable of 10 X, 25X, 40X and 60X magnifications. Thus the effective magnifications possible were 100 X, 250X, 400X and 600X.



1. Reference electrode; 2. Temperature probe; 3. Luggin capillary; 4. Working electrode; 5. Hot plate; 6. Condenser; 7. Bubbler for gas; 8. pH electrode; 9. Counter electrode

Figure 4.1: Schematic of the glass cell (courtesy - Daniel Mosser).

4.1 Electrochemical measurements

All electrochemical measurements were made using a Gamry PC4 monitoring system and analyzed using the accompanying software. First the corrosion potential (E_{corr}) was measured which varied typically from -697 mV to -707 mV. Then the corrosion rate using LPR method was determined and finally the solution resistance was measured with the EIS technique.

The LPR technique is simple and easy to use. It is based on the theoretical and practical experience (Stern²¹, 1959) that the system is not affected and on-line corrosion rate measurements can be taken by converting the corrosion current density (i_{corr}) into corrosion rate. Thus the slope (dE / di_{app}) is measured and i_{corr} is calculated using the Tafel slopes²³ (β_a , β_c , refer to Appendix B for more information).

$$i_{\text{corr}} = \left[\frac{[\beta_a * \beta_c]}{(2.303 * (\beta_a + \beta_c))} \right] * \left(\frac{di_{\text{app}}}{dE} \right) \quad (4.1)$$

where i_{app} is the applied current density, E is the applied voltage. Equation 4.2 shows the conversion between corrosion rate and current density.

$$\text{Corrosion Rate (mm/yr)} = 1.16 * i_{\text{corr}} \quad (4.2)$$

where “ i_{corr} ” is the current density in A/m^2

The LPR measurements were taken at ± 5 mV around the corrosion potential (E_{corr}).

4.2 X-65 mild steel working electrode

The working electrode (WE) was machined from the parent material and had a diameter of 1.2 cm and an area of 5.4 cm^2 . The composition of the X-65 mild steel specimen (as reported by Laboratory Testing Inc.) used in the experiments is as shown in Table 4-1.

Table 4.1: Chemical composition of X-65 steel (wt %)

Al	As	B	C	Ca	Co	Cr	Cu	Mn	Mo	Nb	
0.032	0.005	0.0003	0.05	0.004	0.006	0.042	0.019	1.32	0.031	0.046	
Ni	P	Pb	S	Sb	Si	Sn	Ta	Ti	V	Zr	Fe
0.039	0.013	0.02	0.002	0.011	0.31	0.001	0.007	0.002	0.055	0.003	Rest

4.3 Post-experimental analysis

The X-65 samples were analyzed for the type, protectiveness and thickness of the film formed. All samples were covered with a protective film which was responsible for the reduction in corrosion rates to less than 0.1 mm/yr. In order to expedite results a novel approach was adopted in which the sample was immersed half-way in epoxy for cross-sectioning with the other half used for surface analysis. The advantage of this method is that the metal surface can be examined for localized attack on one side (by removing the film) and SEM analysis can be performed on the side encased in epoxy without having to repeat experiments for each of these two tasks. Also since the two halves are from the same experiment there is better correlation.

Figure 4.2 illustrates the metal sample encased halfway in epoxy and ready for cross-sectional analysis.

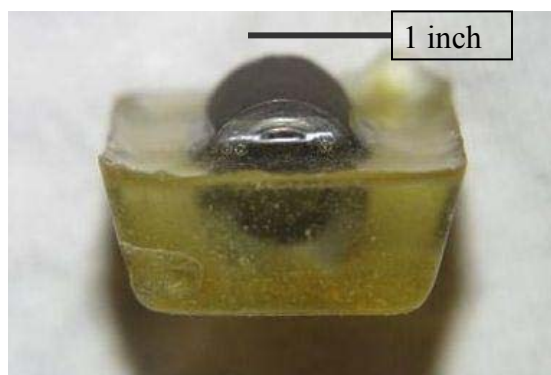


Figure 4.2: Sample encased halfway in epoxy

5. Results

Experiments were carried out at a higher pH as compared to the pH observed in field situations in presence of CO₂ and high temperature in order to facilitate iron carbonate film formation. External addition of iron in the form of Fe²⁺ was also done for the same reason. Experiments containing 50 ppm Fe²⁺ at pH 6.6 reflect SS = 162 and those containing 10 ppm Fe²⁺ at pH 6.6 reflect SS = 32. Similarly at pH 6.3 and pH 6, 50 ppm Fe²⁺ reflects SS = 41 and 10, respectively. The calculation of the SS value at the different pH values and Fe²⁺ concentrations is shown in detail in Appendix E. Experiments were conducted at four SS values 162, 41, 32 and 10. The experiments were divided on the basis of supersaturation (SS) value for better understanding and arranged in decreasing order of SS.

First experiments were started at the highest SS of 162 at pH 6.6 and in the presence of three different free HAc concentrations. In these experiments the pH was kept constant at 6.6 and the Fe²⁺ concentration was fixed at 50 ppm. The total HAc added was 1000, 4000 and 10,000 ppm. Thus, experiments were conducted at SS = 162. The free HAc distribution at pH 6.6 is outlined in Table 5.1 showing that at this pH almost 98% of the acid is in the dissociated acetate form. In the next set of experiments, the Fe²⁺ concentration was changed to 10 ppm which gave a SS of 32 at pH 6.6. This was done to determine the effect of lower SS on film formation in the presence of HAc. The total HAc added was 4000 and 10,000 ppm which at pH 6.6, resulted in free HAc concentrations of 72 and 180 ppm, respectively.

Experiments at SS of 41 and 10 were done only with one total HAc concentration of 1000 ppm. The logic behind these experiments was to determine if change in the SS

value affects film formation in the presence of HAc. Thus at SS of 41 and 10, the free HAc concentration tested for was 35 and 68 ppm respectively as shown in Table 5.2.

Table 5.1: HAc dissociation at fixed pH value

Total HAc /(ppm)	pH	Free [HAc]/(ppm)	[Ac ⁻]/(ppm)
1000	6.6	18	982
4000	6.6	72	3928
10000	6.6	180	9820

Table 5.2: HAc dissociation at different pH values

Total HAc /(ppm)	pH	Free [HAc]/(ppm)	[Ac ⁻]/(ppm)
1000	6.6	18	982
1000	6.3	35	965
1000	6	68	932

5.1 Baseline tests at pH 6.6, stagnant conditions

Baseline experiments were conducted without HAc at 50 and 10 ppm Fe²⁺ each at pH 6.6, to determine the corrosion rates and iron carbonate film formation in the absence of HAc. These experiments will serve as a means of comparison to experiments with HAc.

Figure 5.1 shows the average corrosion rate curves for experiments without HAc at pH 6.6, 80°C, no rotation, with 50 and 10 ppm Fe²⁺. The error bars represent the maximum and minimum values of corrosion rate observed and is applicable for all other graphs wherein the error bars appear. As expected, it takes longer for a protective film to form at

10 ppm Fe^{2+} (SS = 32) than at 50 ppm Fe^{2+} (SS = 162). In both cases, a protective iron carbonate film is formed and the corrosion rate drops rapidly from about 1.3 mm/yr to less than 0.1 mm/yr. This is also reflected in the iron (Fe^{2+}) count taken towards the end of the experiment when it decreased to less than 1 ppm in both cases. Thus it is seen that in this case the change in the Fe^{2+} concentration affects only the rate of film formation, i.e. how fast a protective film is formed not its protectiveness.

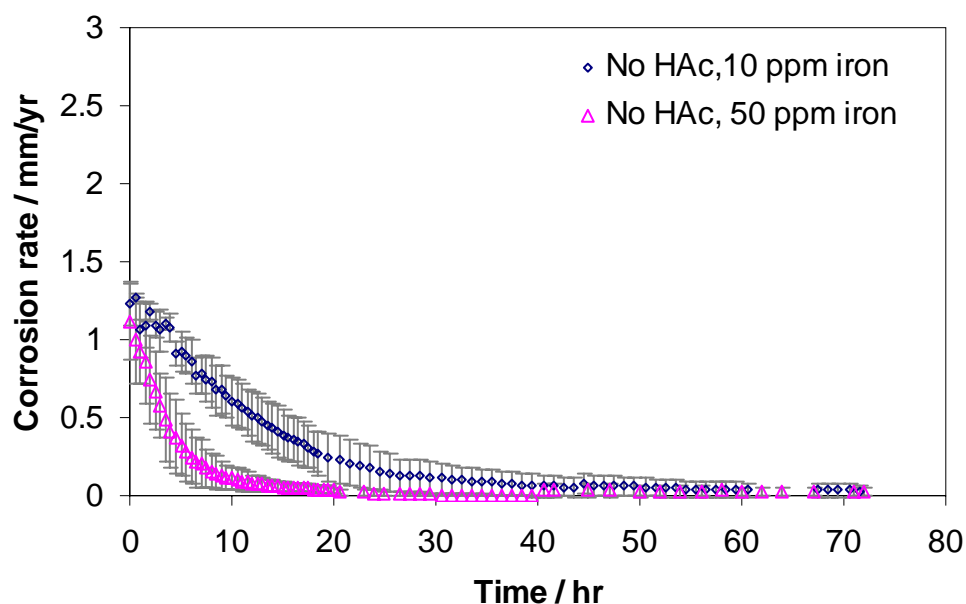


Figure 5.1: Average corrosion rate variation with time in experiments without HAc at pH 6.6, 80°C, 10 and 50 ppm Fe^{2+} , at stagnant pure film formation conditions. (Error bars represent the maximum and minimum values of corrosion rate observed)

5.2 Supersaturation (SS) of 162

a) Without and with 18 ppm free HAc:

Figure 5.2 shows the corrosion rate curves averaged over multiple experiments without and with 18 ppm free HAc at SS = 162, pH 6.6, 80°C, 50 ppm Fe²⁺. Experiments were conducted without and with 18 ppm free HAc over 80 hours until stable results were obtained. Results of three repeatable experiments without and with 18 ppm free HAc are shown. A higher starting corrosion rate is seen in presence of HAc, although HAc has no significant effect on the final corrosion rates. The corrosion rate curves of all experiments performed are shown in the logarithmic scale in Figure 5.3. We see a difference in the final corrosion rates of experiments although they do not have much significance as they are much less than 0.1 mm/yr.

Figure 5.4a shows the SEM front view pictures of the film at 1500X magnification and also the optical microscope pictures at 600X with the film removed (refer to Appendix F for more details) to examine for evidence of localized attack. As seen from the optical microscope pictures in Figure 5.4b, there is uniform corrosion on the metal and no evidence of localized attack is observed. Figure 5.5 shows the SEM cross-section pictures at 500X. There is no differentiation possible between the thickness of films formed without and with 18 ppm free HAc. The films in both cases are 10-15 μm thick which shows that presence of HAc has no effect on film thickness and protectiveness in these conditions.

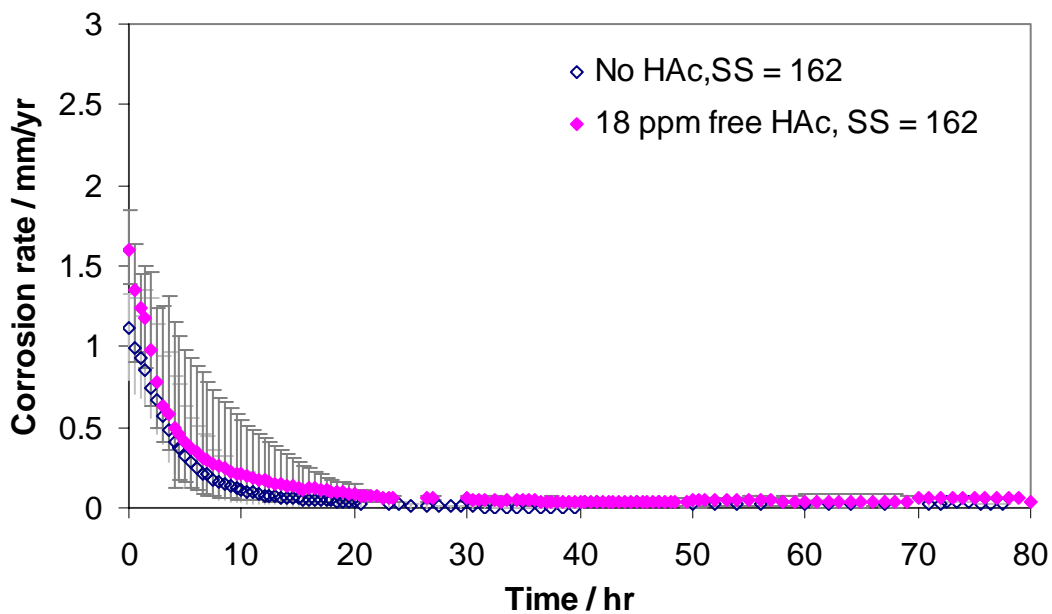


Figure 5.2: Average corrosion rate plot with time in experiments without and with 18 ppm free HAc (1000 ppm total) at SS = 162, pH 6.6, 80°C, 50 ppm Fe²⁺. (Error bars represent the maximum and minimum values of corrosion rate observed, refer to Figure 5.3 for the curves in the logarithmic scale, 5.4 for SEM front view and 5.5 for SEM cross-sectional view.)

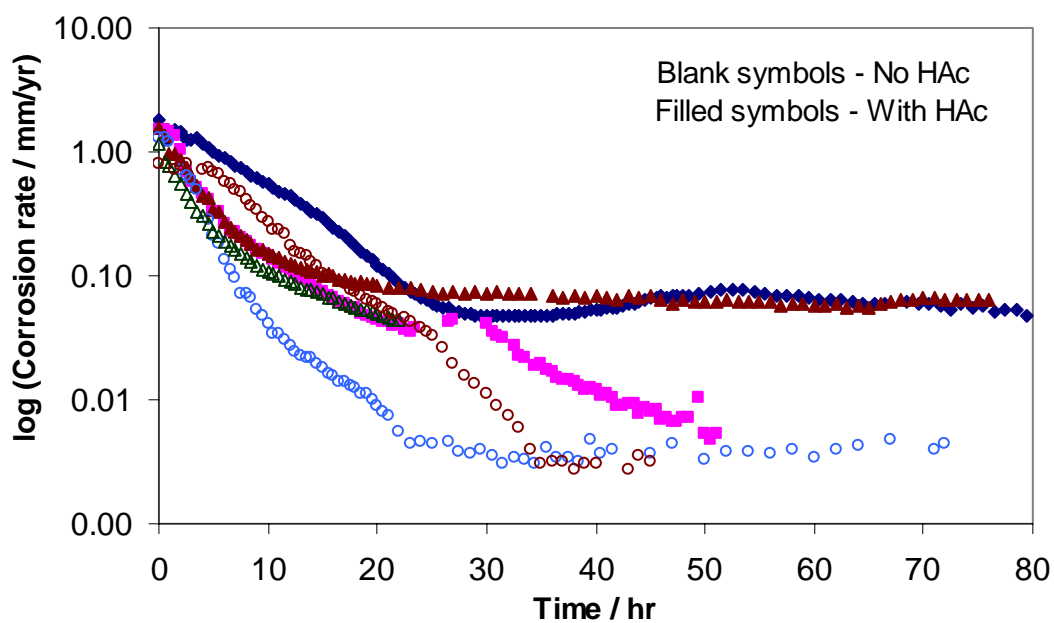
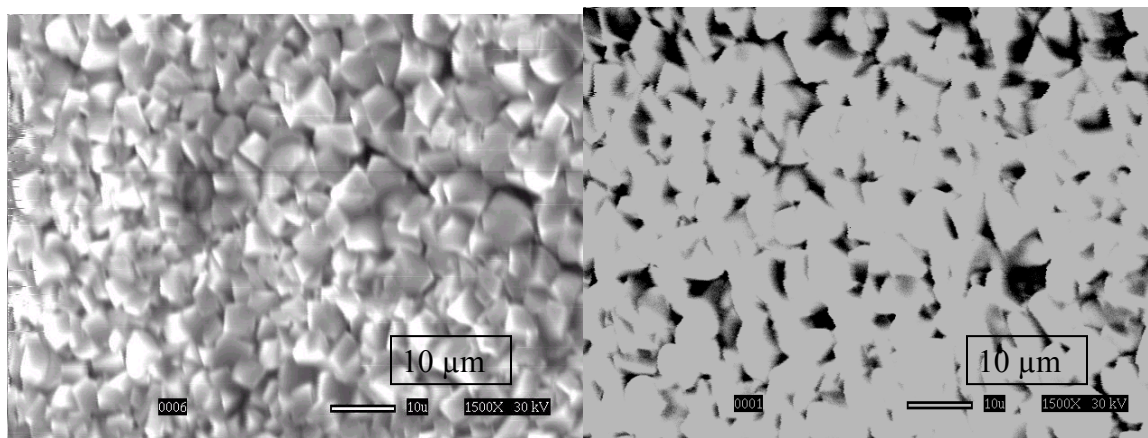


Figure 5.3: Corrosion rate progression with time in the logarithmic scale at SS = 162, pH 6.6, $T = 80^{\circ}\text{C}$, 50 ppm Fe^{2+} , without and with 18 ppm free HAc, stagnant conditions. (Refer to Figure 5.2 for the average curves, 5.4 for SEM front view and 5.5 for SEM cross-sectional view.)

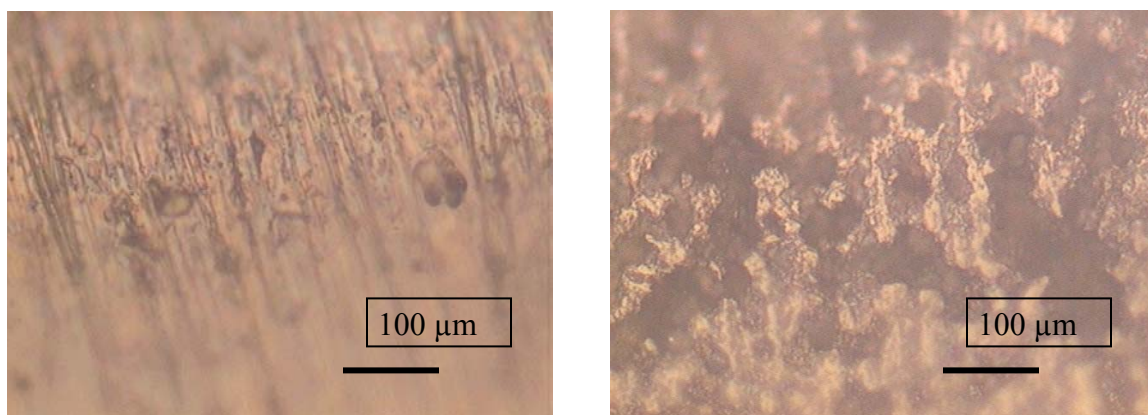
a) SEM pictures (frontal view) at 1500 X



Without HAC

With 18 ppm free HAC

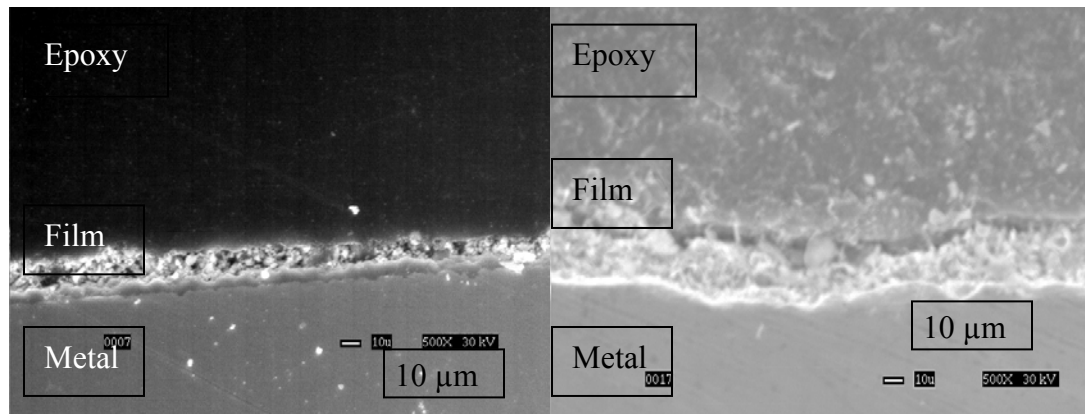
b) Optical microscope pictures at 600X



Film removed (without HAC)

Film removed (with 18 ppm free HAC)

Figure 5.4: Front view pictures of FeCO_3 film at SS = 162, pH 6.6, 80°C, 50 ppm Fe^{2+} , without and with 18 ppm free HAC, stagnant condition. (Refer to Figure 5.2 for the average curves, 5.3 for all the curves on the logarithmic scale, 5.5 for SEM cross-sectional view.)



Without HAC

With 18 ppm free HAC

Figure 5.5: SEM pictures (cross sectional view) of FeCO_3 film at 500X, SS = 162, pH 6.6, 80° C, 50 ppm Fe^{2+} , 18 ppm free HAC, stagnant condition. (Refer to Figure 5.2 for the average curves, 5.3 for all the curves on the logarithmic scale, 5.4 for SEM front view)

b) Without and with 72 ppm free HAC:

Figure 5.6 shows the corrosion rate curves averaged over the multiple experiments without and with 72 ppm free HAC at SS = 162, pH 6.6, 80°C, 50 ppm Fe^{2+} . Experiments were conducted without and with 72 ppm free HAC over 3 days until stable results were obtained. We again see a higher starting corrosion rate in the presence of HAC although HAC has no significant effect on the final corrosion rates. The experimental curves of all experiments performed are shown on the logarithmic scale in Figure 5.7 which shows a slight difference in the corrosion rate progression. On examination of the front view pictures of the film as shown in Figure 5.8a at 1500X it is seen that the size of the crystals with HAC is greater than those observed without HAC, although both offered the same

protection. The optical microscope pictures with the film removed as shown in Figure 5.8b show no evidence of localized attack.

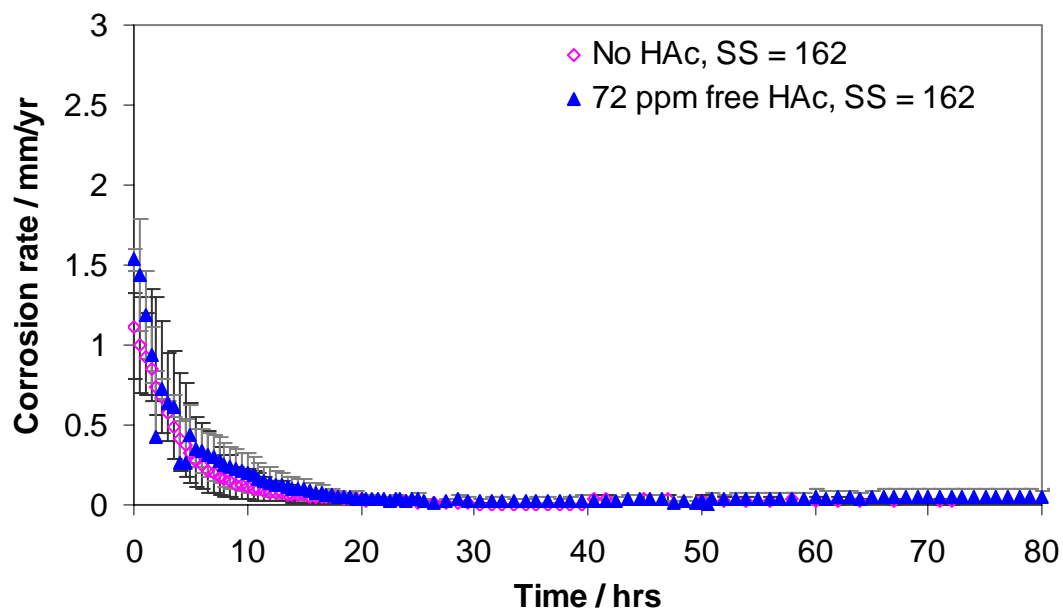


Figure 5.6: Average corrosion rate plot with time in experiments without and with 72 ppm free HAc (4000 ppm HAc total) at SS = 162, pH 6.6, 80° C, 50 ppm Fe²⁺(Error bars represent the maximum and minimum values of corrosion rate observed, refer to Figure 5.7 for the curves in the logarithmic scale, 5.8 for SEM front view and 5.9 for SEM cross-sectional view.)

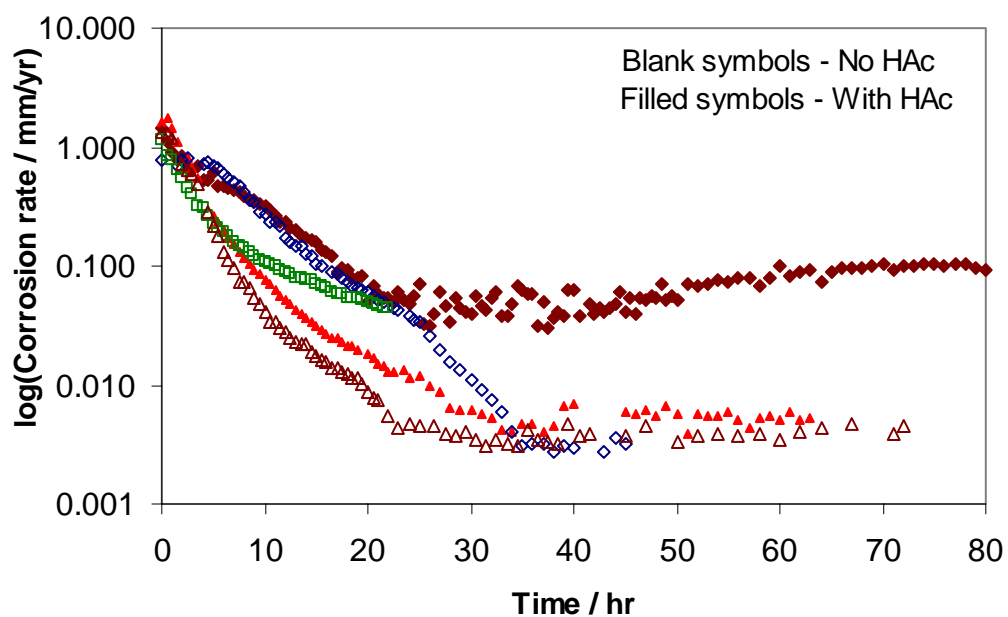
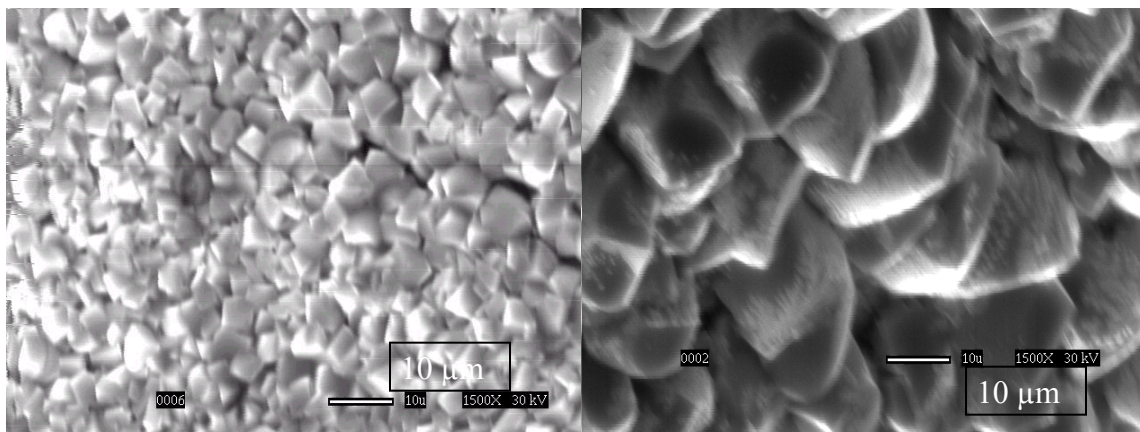


Figure 5.7: Corrosion rate progression with time in the logarithmic scale at SS = 162, pH 6.6, $T = 80^{\circ}\text{C}$, 50 ppm Fe^{2+} , without and with 72 ppm free HAC, stagnant conditions. (Refer to Figure 5.6 for the average curves, 5.8 for the front view and 5.9 for SEM cross-sectional view)

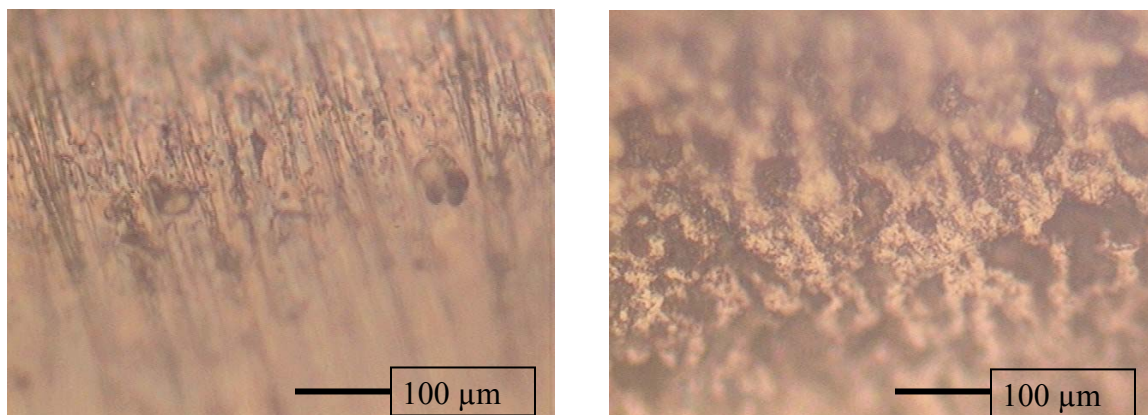
a) SEM pictures (frontal view) at 1500 X



Without HAC

With 72 ppm free HAC

b) Optical microscope pictures at 600X



Film removed (without HAC)

Film removed (with 72 ppm free HAC)

Figure 5.8: Front view pictures of FeCO_3 film at SS = 162, pH 6.6, 80°C, 50 ppm Fe^{2+} , without and with 72 ppm free HAC, stagnant condition. (Refer to Figure 5.6 for the average curves, 5.7 for the curves in the logarithmic scale, 5.9 for the cross-sectional view)

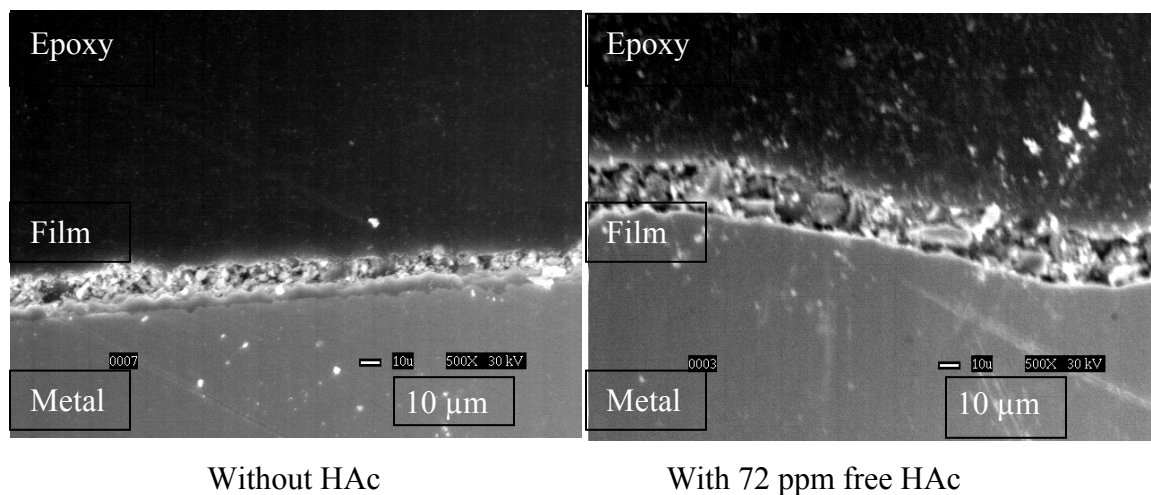


Figure 5.9: SEM pictures (cross sectional view) of FeCO_3 film at 500 X, SS = 162, pH 6.6, 80°C, 50 ppm Fe^{2+} , with 72 ppm free HAc, stagnant condition. (Refer to Figure 5.6 for the average curves, 5.7 for the curves in the logarithmic scale, 5.8 for the front view.)

Figure 5.9 shows the SEM cross-section pictures at 500X. The films in both cases are 15-25 μm thick which shows that the presence of 72 ppm free HAc has no effect on film thickness and protectiveness.

c) Without and with 180 ppm free HAc:

Figure 5.10 shows average corrosion rate curves for experiments without and with 180 ppm free HAc at pH 6.6, 80°C, 50 ppm Fe^{2+} . The starting corrosion rate with HAc is again higher than experiments without HAc although there is no effect on the final corrosion rates. The experimental curves of all experiments performed are shown on a logarithmic scale in Figure 5.11.

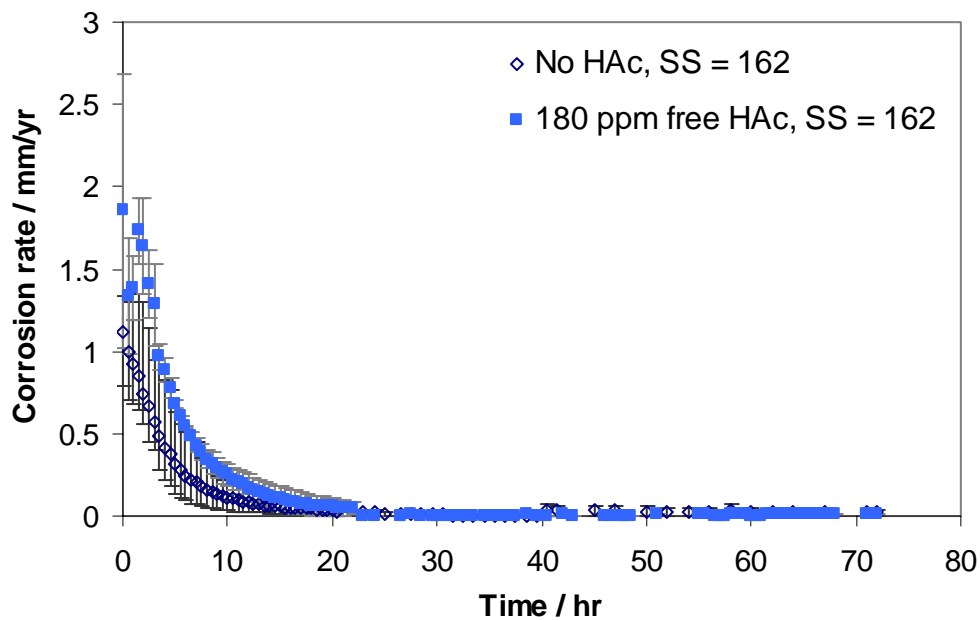


Figure 5.10: Average corrosion rate plot with time in experiments without and with 180 ppm free HAc (10,000 ppm HAc total) at SS = 162, pH 6.6, 80°C, 50 ppm Fe^{2+} (Error bars represent the maximum and minimum values of corrosion rate observed, refer to Figure 5.11 for the curves in the logarithmic scale, 5.12 for SEM front view and 5.13 for SEM cross-sectional view.)

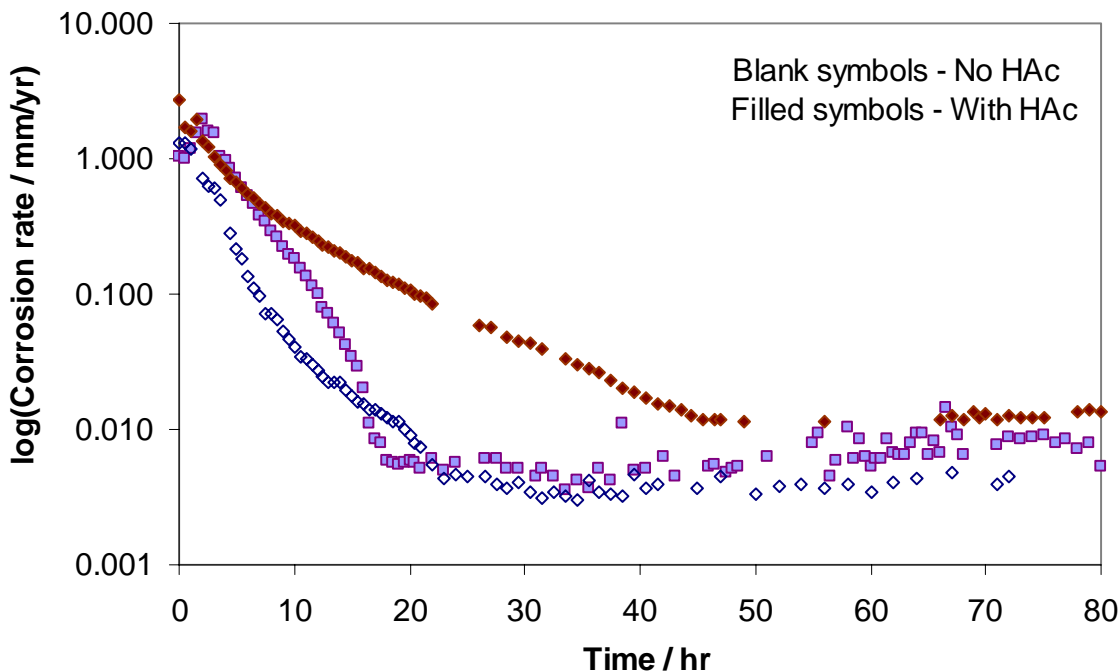


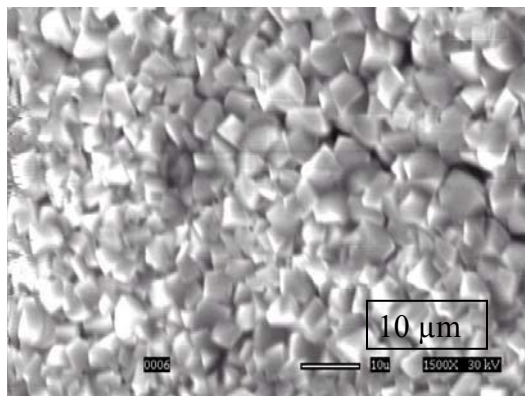
Figure 5.11: Corrosion rate progression with time in the logarithmic scale at pH 6.6, $T = 80^{\circ}\text{C}$, 50 ppm Fe^{2+} , without and with 180 ppm free HAC, stagnant conditions. (Refer to Figure 5.10 for the average curves, 5.12 for SEM front view and 5.13 for SEM cross-sectional view)

There is again a slight variation in corrosion rates but it must be noted that these are insignificant as they are in the logarithmic scale. Figure 5.12a shows the front view pictures of the film at 1500X and also with the film removed at 600X to look for localized attack. The size of crystals with HAC is similar to those observed without HAC. We also see from the optical microscope pictures as in Figure 5.12b, there is no localized attack. Figure 5.13 shows the SEM cross-section pictures at 500X. Again the thicknesses of films formed without and with HAC are identical.

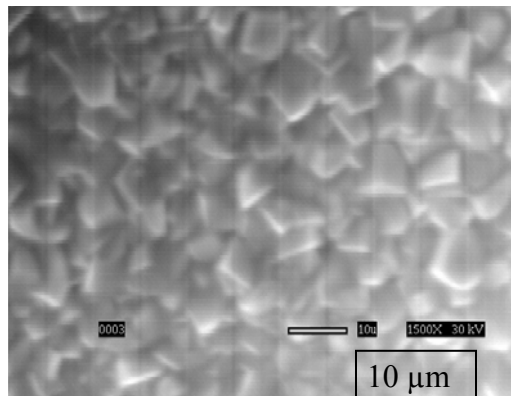
Figure 5.14 shows the average curve comparison at SS = 162, pH 6.6, without and with 18, 72 and 180 ppm free HAC over 3 days in the logarithmic scale. We see a variation in

the corrosion rates but there is no direct relation between HAc concentration and corrosion rate.

a) SEM pictures (frontal view) at 1500 X

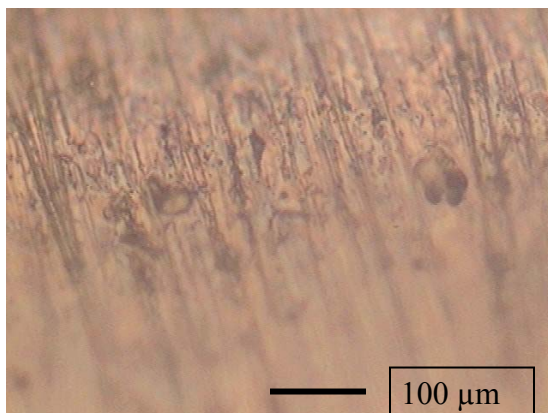


Without HAc

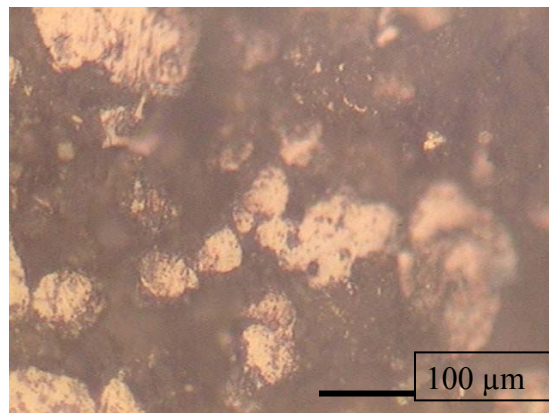


With 180 ppm free HAc

b) Optical microscope pictures at 600X

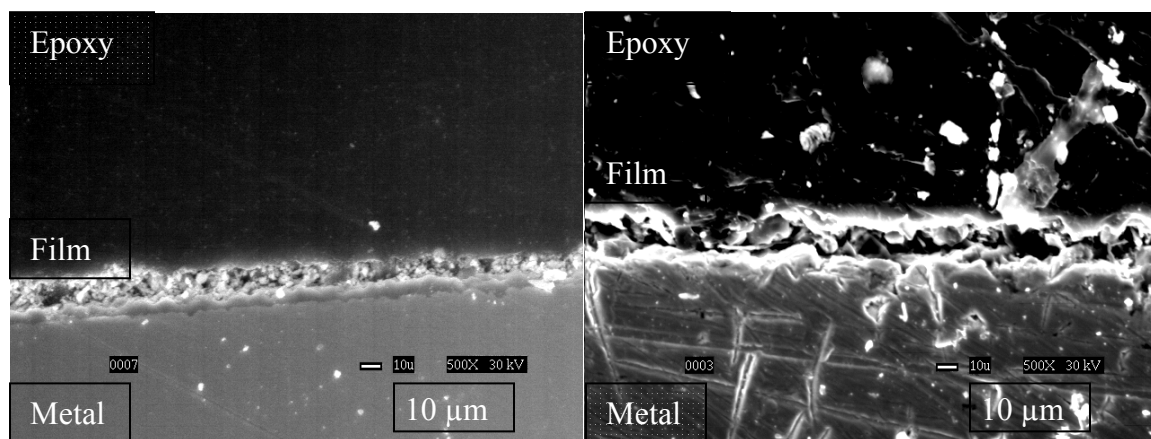


Film removed (without HAc)



Film removed (with 180 ppm free HAc)

Figure 5.12: Front view pictures of FeCO₃ film at SS = 162, pH 6.6, 80°C, 50 ppm Fe²⁺, without and with 180 ppm free HAc, stagnant condition. (Refer to Figure 5.10 for the average curves, 5.11 for the curves in the logarithmic scale, 5.13 for SEM cross-sectional view)



Without HAC

With 180 ppm free HAC

Figure 5.13: SEM pictures (cross sectional view) of FeCO_3 film at 500 X, SS = 162, pH 6.6, 80°C, 50 ppm Fe^{2+} , 180 ppm free HAC, stagnant condition. (Refer to Figure 5.10 for the average curves, 5.11 for the curves in the logarithmic scale, 5.12 for the front view)

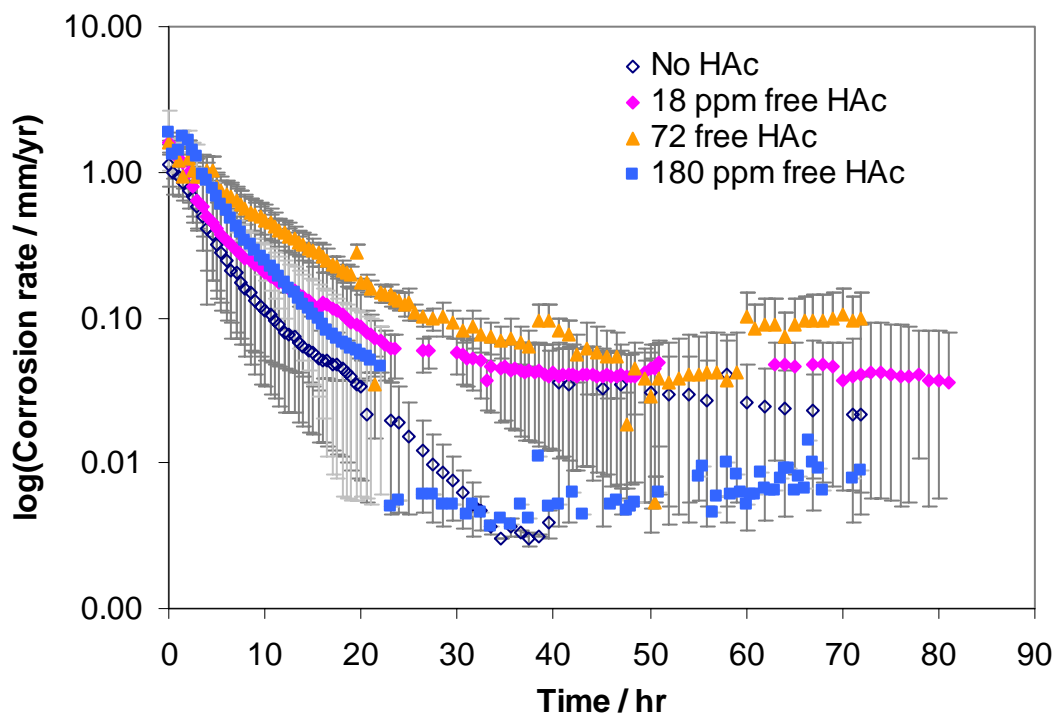


Figure 5.14: Comparison of the average curves at SS = 162, pH 6.6, 80°C, 50 ppm Fe^{2+} , with 18, 72 and 180 ppm free HAc, stagnant condition. (Error bars represent the maximum and minimum values of corrosion rates observed)

5.2.1 Film integrity experiments at supersaturation (SS) of 162

Experiments were carried out at pH 6.6, 50 ppm Fe^{2+} (SS = 162), without and with 72 ppm free HAc, at 0 and 9000 rpm to determine integrity of film. The rotational speed was set using a Pine Instruments speed control unit. A protective film was grown on the stagnant sample (which was indicated by the corrosion rate being less than 0.1 mm/yr), then the sample was rotated at 9000 rpm (~ 5.6 m/sec peripheral velocity in the RCE assembly) to see effect of rotation without and with HAc. The shear stress (τ) calculated at 9000 rpm in the RCE assembly was 50 Pa. Experiments were done

upto 100 hours, some shorter to see long term effects. Figure 5.15 shows the corrosion rate progression with time in two different rotation experiments without HAc.

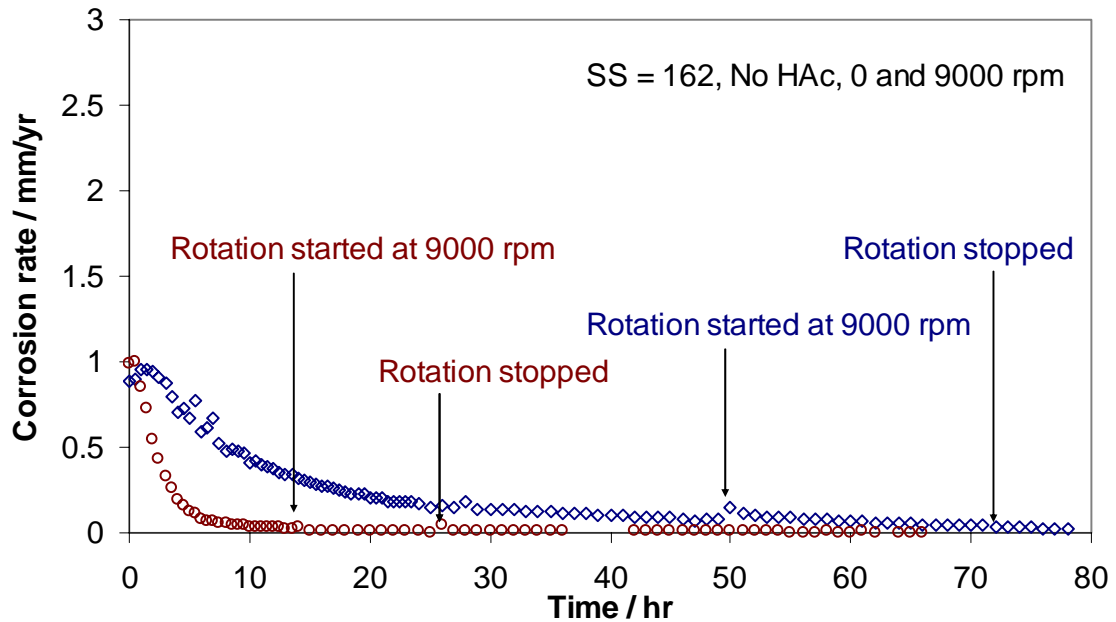


Figure 5.15: Corrosion rate variation with time in rotation experiments at SS = 162, 0 and 9000 rpm without HAc at pH 6.6, 80°C, 50 ppm Fe²⁺. (Refer to Figure 5.16 for curves in the logarithmic scale)

There is no significant effect of starting rotation on the corrosion rates once a protective film has been formed. Refer to Figure 5.16 where the same curves are shown in a logarithmic scale. The corrosion rate increases slightly when rotation is started but then starts to decrease. Figure 5.17 shows the corrosion rate progression with time in two different experiments with 72 ppm free HAc. Figure 5.18 shows the same curves in the logarithmic scale. We see that in the presence of HAc, rotation hardly affects the corrosion rates.

Figure 5.19 compares the front view images of the film at 1500X without and with 72 ppm free HAc. We see that rotation has no effect on integrity of the film. The cross-section pictures at 500X also tell the same story as shown in Figure 5.20.

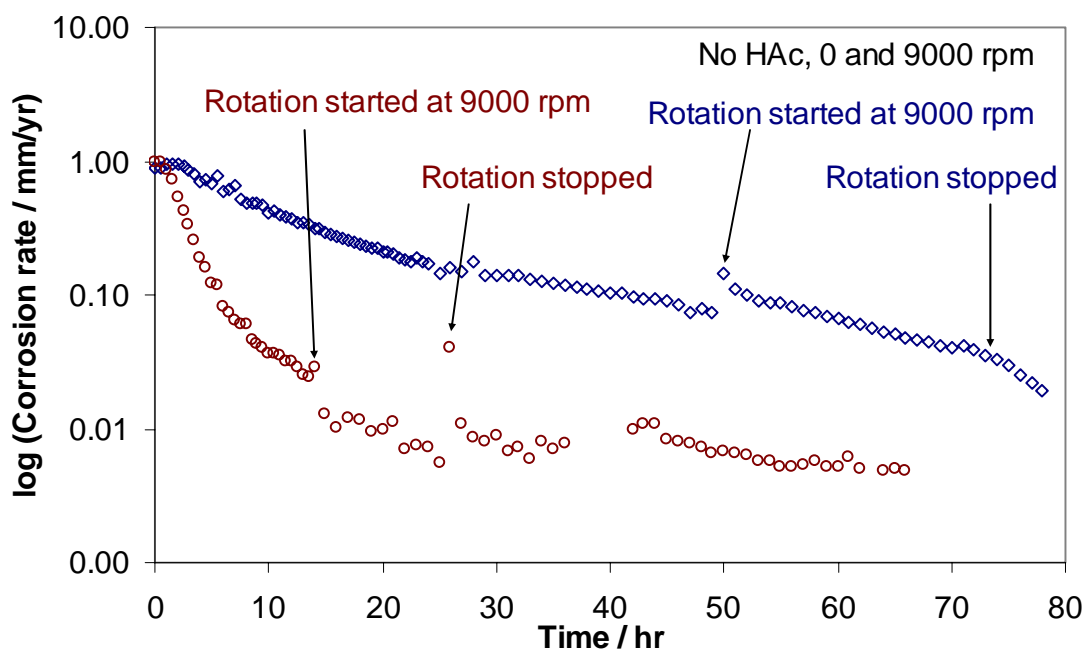


Figure 5.16: Corrosion rate progression with time in the logarithmic scale at SS = 162, pH 6.6, T = 80°C, 50 ppm Fe²⁺, without HAc, stagnant and 9000 rpm conditions. (Refer to Figure 5.15 for curves in the normal scale)

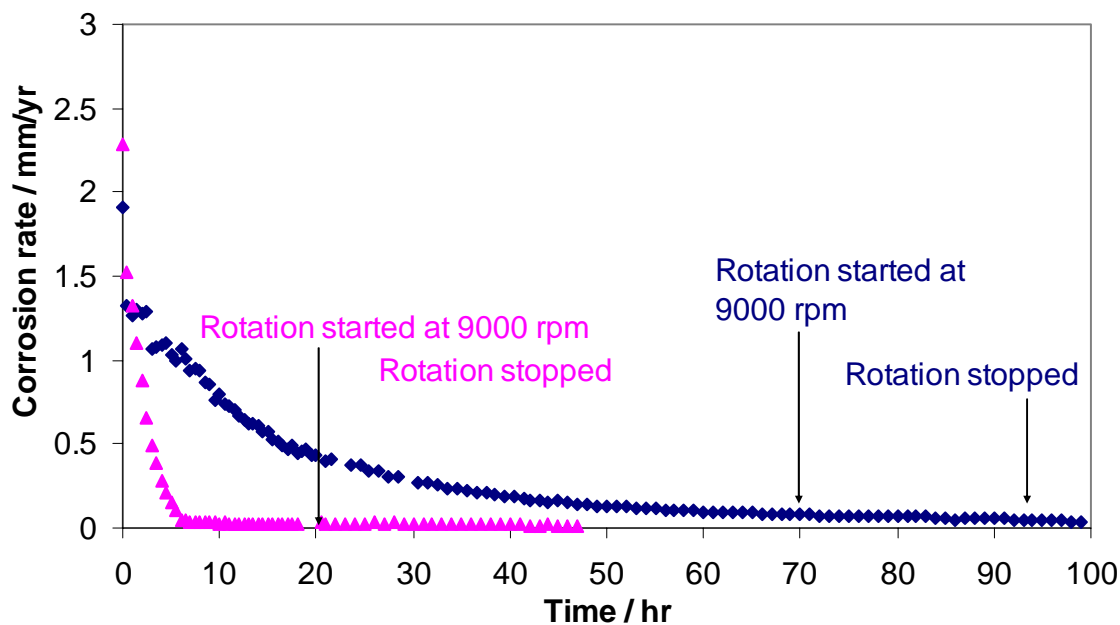


Figure 5.17: Corrosion rate variation with time in rotation experiments at SS= 162, 0 and 9000 rpm with 72ppm free HAc at pH 6.6, 80°C, 50 ppm Fe²⁺. (Refer to Figure 5.18 for curves in the logarithmic scale)

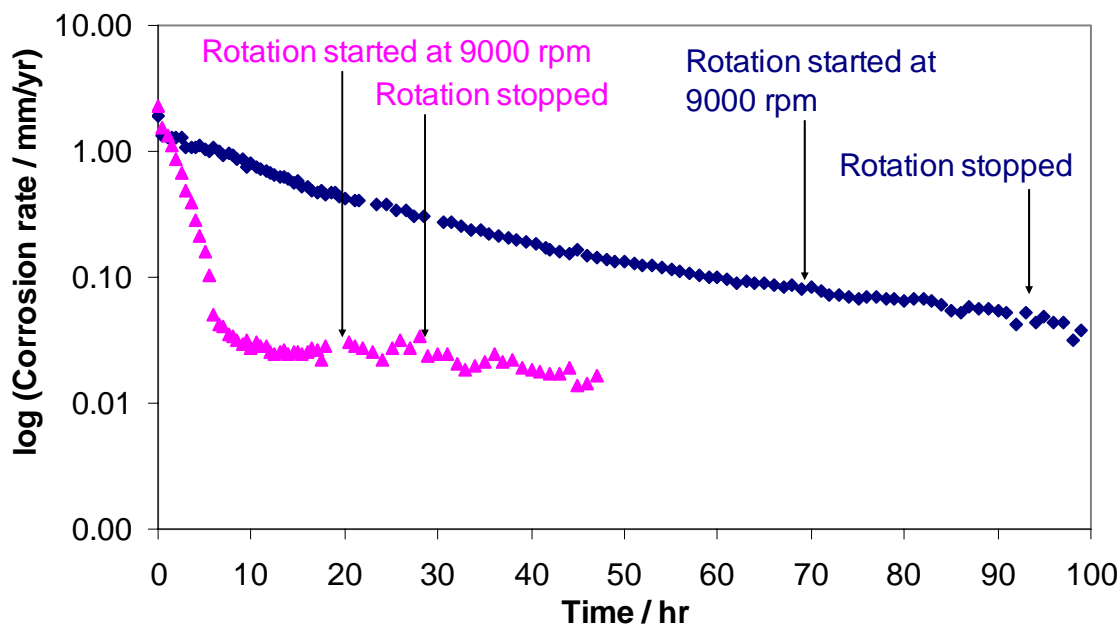
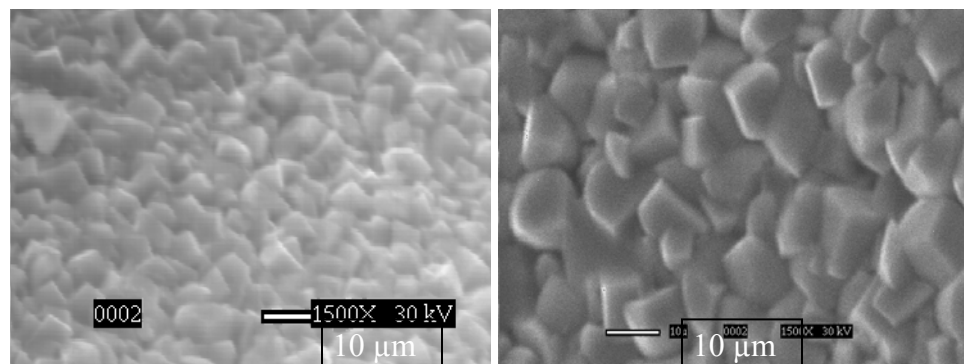


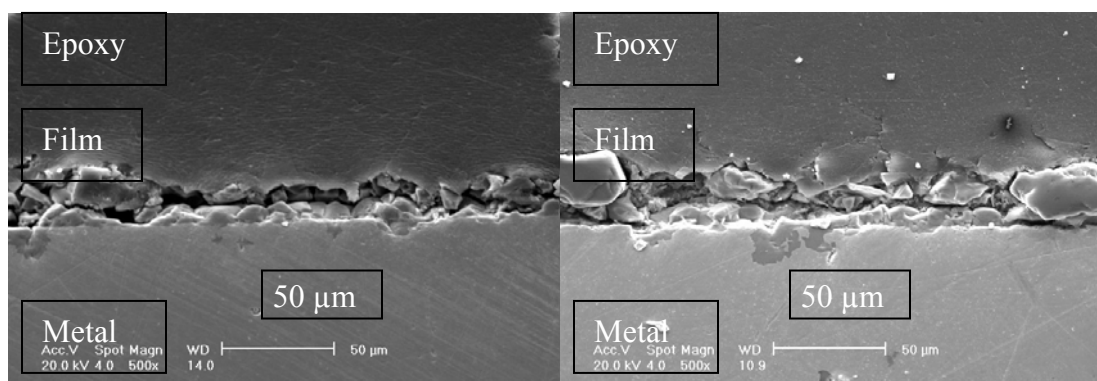
Figure 5.18: Corrosion rate progression with time in the logarithmic scale at SS = 162, pH 6.6, T = 80°C, 50 ppm Fe²⁺, with 72 ppm free HAc, stagnant and 9000 rpm conditions. (Refer to Figure 5.17 for curves in the normal scale)



Without HAC

With 72 ppm free HAC

Figure 5.19: SEM pictures (frontal view) of FeCO_3 film at SS = 162, pH 6.6, 80°C, 50 ppm Fe^{2+} , 0 and 9000 rpm condition at 1500 X. (Refer to Figure 5.20 for SEM cross-section pictures.)



Without HAC

With 72 ppm free HAC

Figure 5.20: SEM pictures (cross sectional view) of FeCO_3 film at 500 X, SS = 162, pH 6.6, 80°C, 50 ppm Fe^{2+} , 0 and 9000 rpm. (Refer to Figure 5.19 for SEM front view pictures.)

5.3 Supersaturation (SS) of 41

Without and with 68 ppm free HAc:

The experimental procedure was repeated at pH 6.3 (a less favorable condition for FeCO_3 film to form, SS = 41 and more free HAc) and the average corrosion rates progression with time both without and with 68 ppm free HAc were plotted. Figure 5.21 shows the average curves without and with 68 ppm free HAc. The corrosion rate starts to drop from about 1.7 mm/yr to less 0.5 mm/yr within 20 hrs in experiments with 68 ppm free HAc. But again there is no significant effect of HAc on the corrosion rate. Figure 5.22 shows the curves of all experiments conducted in the logarithmic scale. We see that the curves without and with HAc are very similar to each other. Figure 5.23 depicts the SEM pictures (frontal view) of FeCO_3 film at pH 6.3 without and with HAc at 1500 X. There is no difference in the FeCO_3 crystal size and the presence of HAc does not affect film formation. The SEM pictures (cross sectional view) of FeCO_3 film at pH 6.3, without and with HAc at 500 X are shown in Figure 5.24. In the experiment without HAc we see a thicker film (~ 40 μm) than compared to the 15 μm film that we see with 35 ppm free HAc. But, as regards to the protectiveness of the thinner film with HAc, we see that it is unaffected as evident from the corrosion rate drop below 0.1 mm/yr as shown in Figure 5.21.

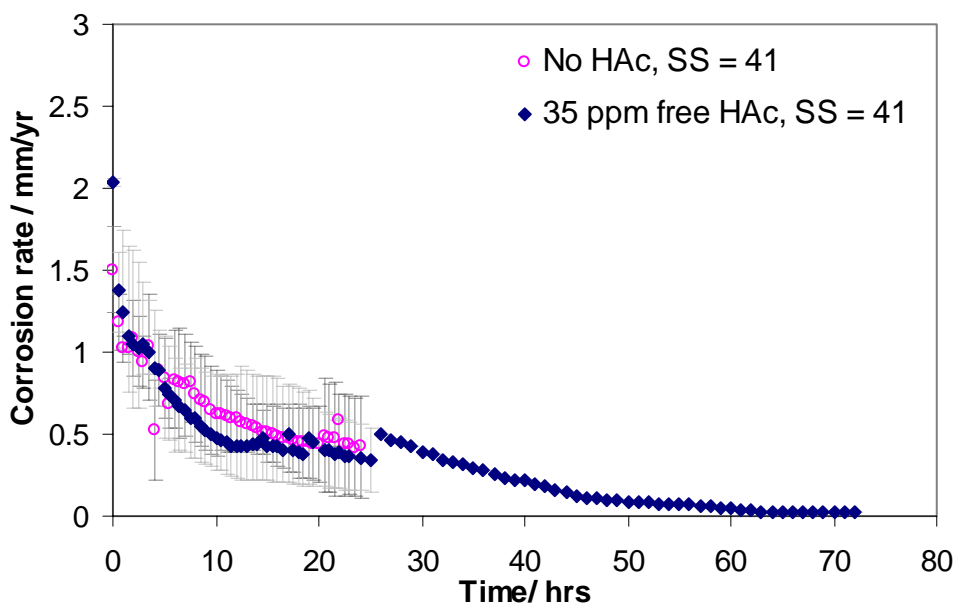


Figure 5.21: Average corrosion rate with time in experiments with and without 35 ppm free HAc (1000 ppm HAc total) at SS = 41, pH 6.3, 80°C, 50 ppm Fe²⁺ (Error bars represent the maximum and minimum values of corrosion rate observed, refer to Figure 5.22 for the curves in the logarithmic scale, 5.23 for SEM front view and 5.24 for SEM cross-sectional view.)

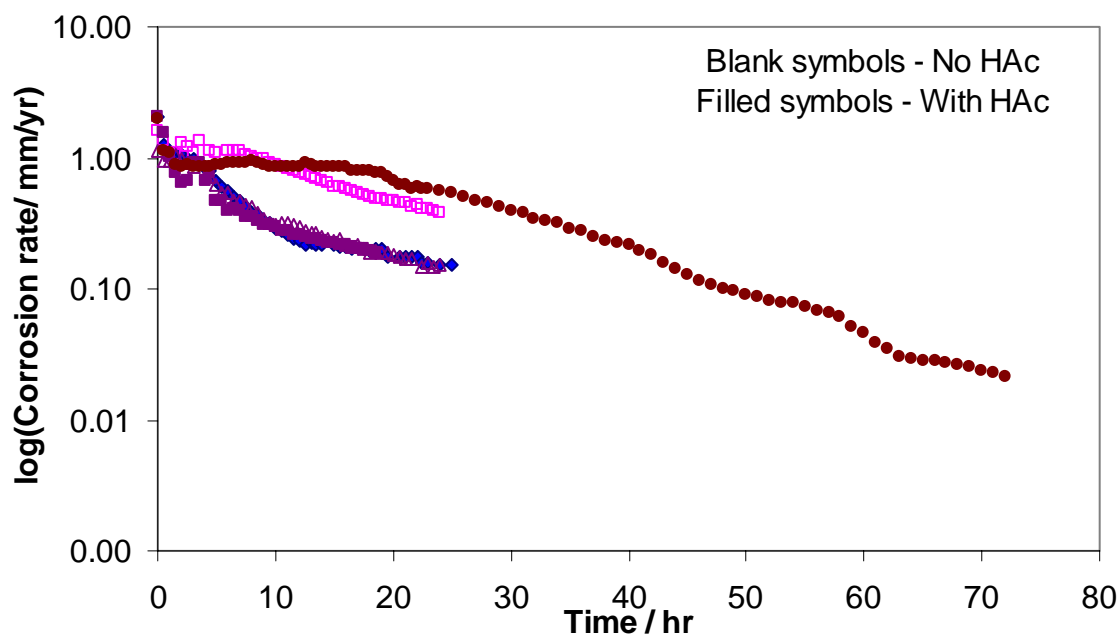
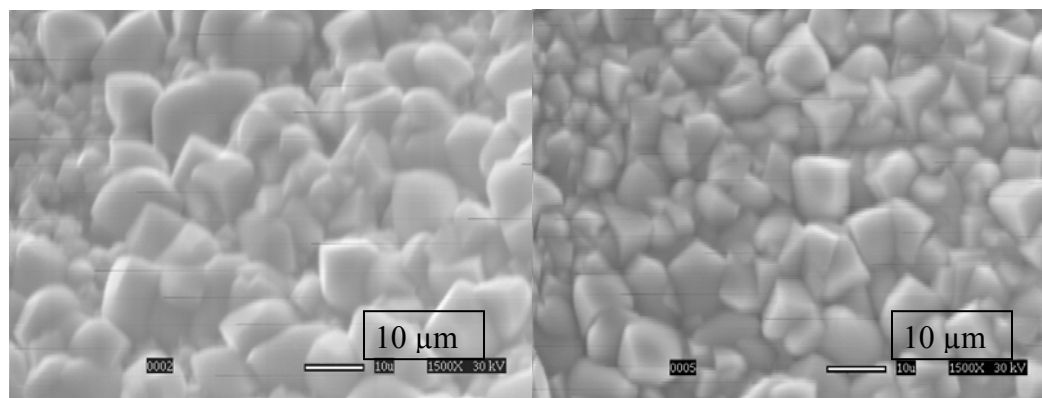


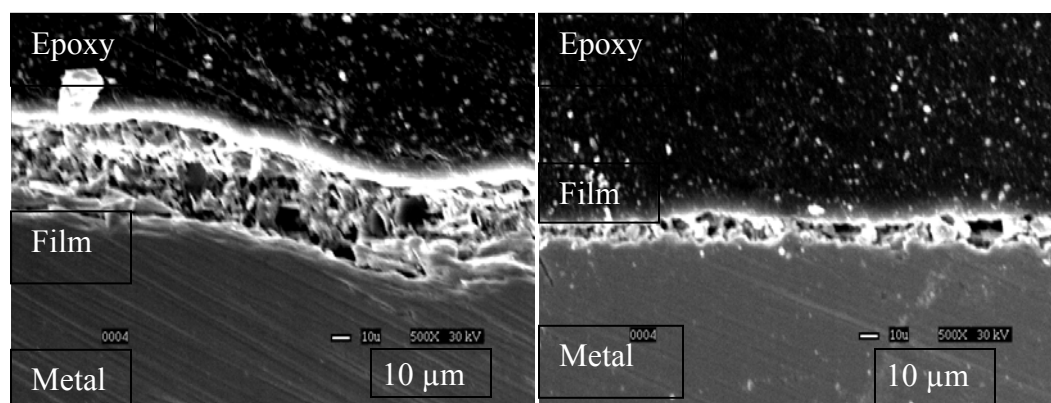
Figure 5.22: Corrosion rate progression with time in the logarithmic scale at SS = 41, pH 6.3, T = 80°C, 50 ppm Fe²⁺, without and with 35 ppm free HAC, stagnant conditions. (Refer to Figure 5.21 for the average curves, 5.23 for SEM front view and 5.24 for SEM cross-sectional view.)



Without HAC

With 35 ppm free HAC

Figure 5.23: SEM pictures (frontal view) at 1500 X of FeCO₃ film at SS = 41, pH 6.3, 80°C, 50 ppm Fe²⁺, stagnant condition. (Refer to Figure 5.21 for the average curves, 5.22 for the curves in the logarithmic scale, 5.24 for SEM cross-sectional view.)



Without HAC

With 35 ppm free HAC

Figure 5.24: SEM pictures (cross sectional view) of FeCO_3 film at 500 X, pH 6.3, 80°C , 50 ppm Fe^{2+} , stagnant condition. (Refer to Figure 5.21 for the average curves, 5.22 for the curves in the logarithmic scale, 5.23 for SEM front view.)

5.4 Supersaturation (SS) of 32

a) Without and with 72 ppm free HAC:

Now let us see the results at an even lower SS, i.e. even less favorable conditions for film formation. Figure 5.25 shows average corrosion rate curves for experiments at SS = 32, pH 6.3, 10 ppm Fe^{2+} , stagnant condition without and with 72 ppm free HAC, over 3 days. From the figure, there is no significant effect of HAC after 30 hours although the starting corrosion rates with HAC are higher. Refer to Figure 5.26 for the corrosion rates of all experiments conducted in the logarithmic scale at the same conditions. Figure 5.27a shows the front view pictures of the film at 1500X and also with the film removed at 600X to look for localized attack. The size of crystals is also the same as compared to those observed without HAC. There is no evidence of localized attack as seen from Figure 5.27b. Figure 5.28 shows the SEM cross-section pictures at 500X. Again the thicknesses of films formed without and with HAC are similar.

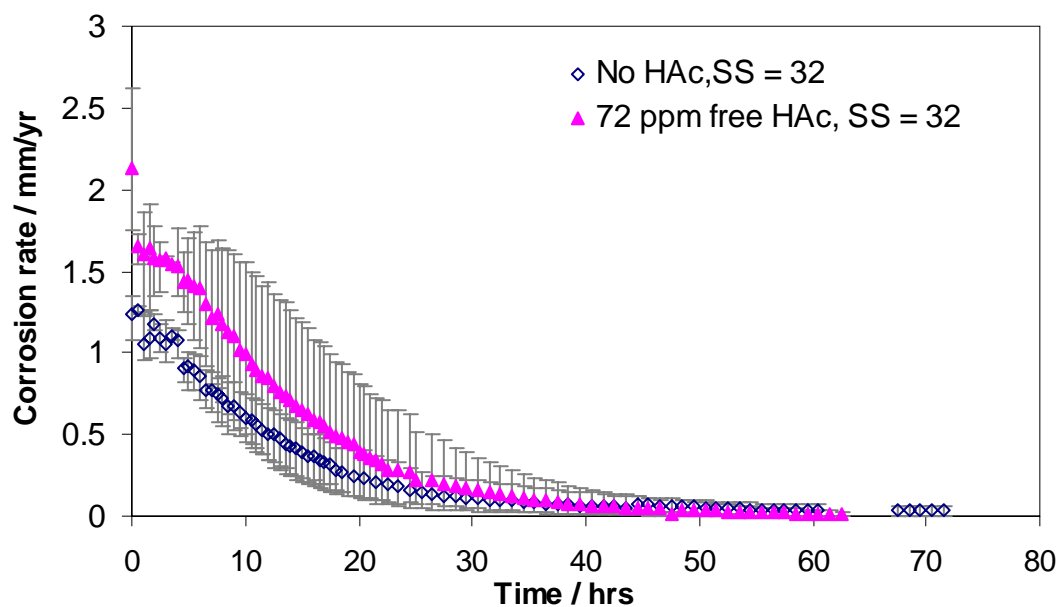


Figure 5.25: Average corrosion rate variation with time in experiments without and with 72ppm free HAc (4000 ppm HAc total) at SS = 32, pH 6.6, 80°C, 10 ppm Fe²⁺. (Error bars represent the maximum and minimum values of corrosion rate observed, refer to Figure 5.26 for the curves in the logarithmic scale, 5.27 for SEM front view and 5.28 for SEM cross-sectional view.)

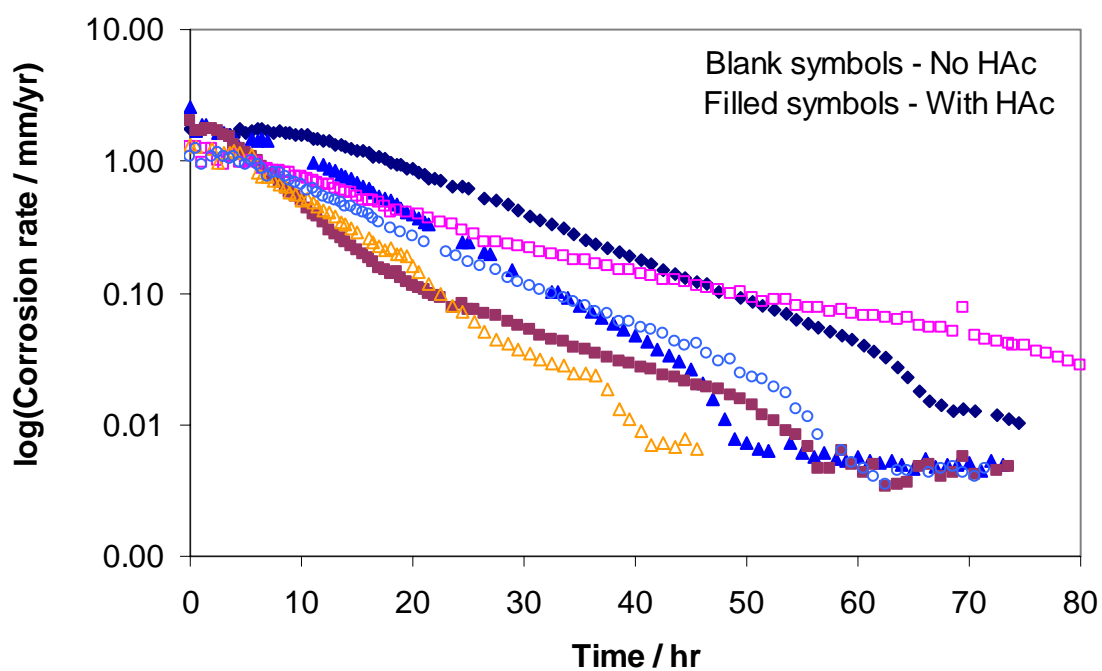
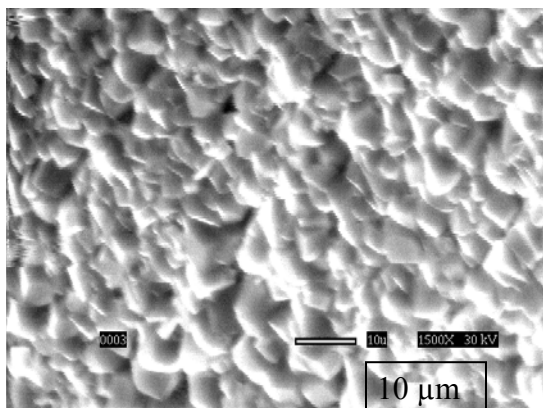
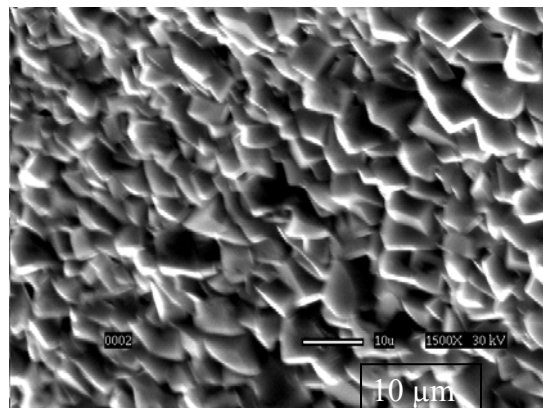


Figure 5.26: Corrosion rate progression with time in the logarithmic scale at SS = 32, pH 6.6, T = 80°C, 10 ppm Fe²⁺, without and with 72 ppm free HAC, stagnant conditions. (Refer to Figure 5.25 for the average curves, 5.27 for SEM front view and 5.28 for SEM cross-sectional view.)

a) SEM pictures (frontal view) at 1500 X

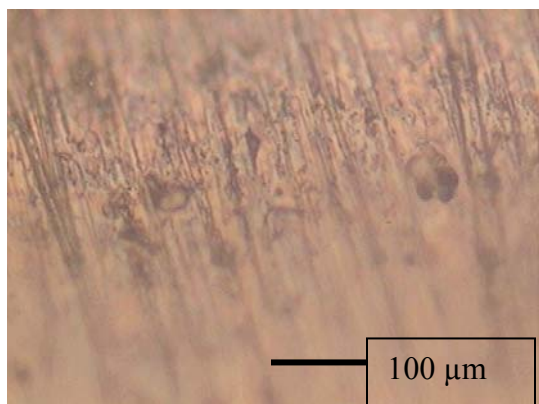


Without HAC

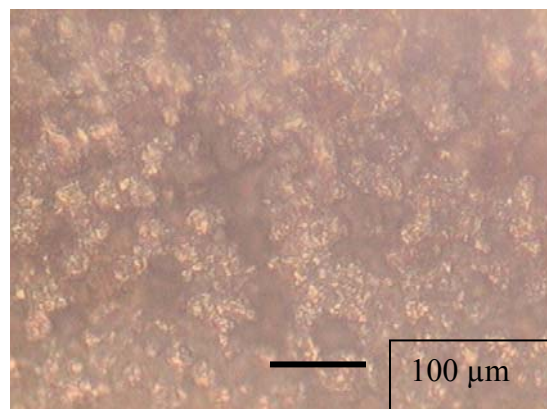


With 72 ppm free HAC

b) Optical microscope pictures at 600X

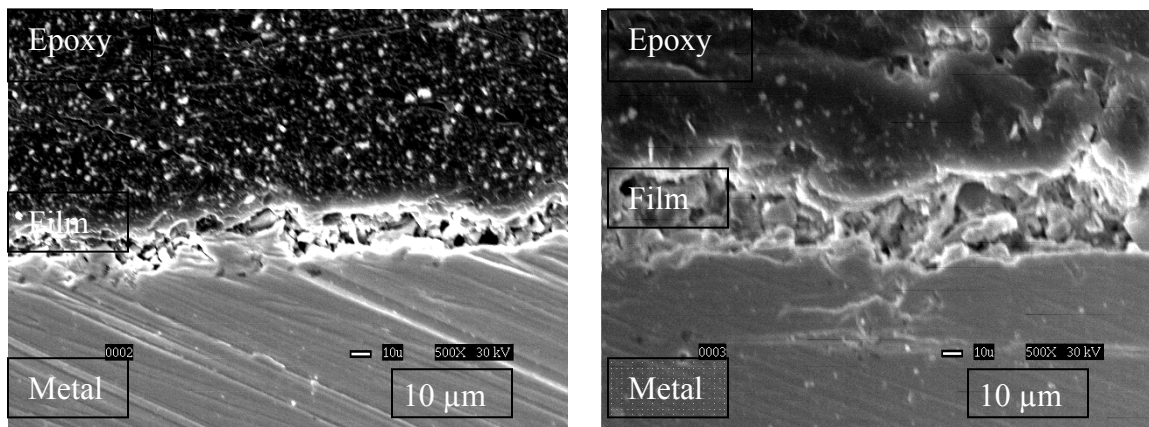


Film removed (without HAC)



Film removed (with 72 ppm free HAC)

Figure 5.27: Front view pictures of FeCO₃ film at SS = 32, pH 6.6, 80°C, 10 ppm Fe²⁺, without and with 72 ppm free HAC, stagnant condition. (Refer to Figure 5.25 for the average curves, 5.26 for curves in the logarithmic scale, 5.28 for SEM cross-sectional view.)



Without HAC

With 72 ppm free HAC

Figure 5.28: SEM pictures (cross sectional view) of FeCO_3 film at 500 X, SS = 32, pH 6.6, 80°C, 10 ppm Fe^{2+} , 72 ppm free HAC, stagnant condition. Refer to Figure 5.25 for the average curves, 5.26 for curves in the logarithmic scale, 5.27 for SEM front view.)

Figure 5.29 shows the average corrosion rates with time for two repeatable experiments each without and with 180 ppm free HAC at SS = 32, pH 6.6, 80°C, 10 ppm Fe^{2+} . The starting corrosion rate with 180 ppm free HAC is higher than that without HAC suggesting that there is a slight effect of HAC at this SS on the time required to form a protective film not on the film protectiveness.

Refer to Figure 5.30 for the corrosion rates of all experiments without and with HAC on a logarithmic scale.

Figure 5.31a shows the front view pictures of the film at 1500X and also with the film removed at 600X to look for localized attack. The size of crystals is larger than those observed without HAC although both offered similar corrosion protection. No evidence of

localized attack is observed as seen from Figure 5.31b. Figure 5.32 shows the SEM cross-section pictures at 500X. Again the thicknesses of films formed without and with HAc are identical.

Figure 5.33 shows the comparison of the average curves at SS = 32, without and with 72 and 180 ppm free HAc in the logarithmic scale. There is not much difference in the corrosion rates with 72 ppm free HAc and 180 ppm free HAc.

Measurement of film thickness using weight loss method:

The weight of the film was measured in experiments without HAc at SS = 162 and SS = 32 at pH 6.6 and an estimate of the film thicknesses were obtained. ASTM Standard Practice G1²², using Clarke's solution was followed. Taking¹⁹ a density of FeCO₃ of 3960 kg/m³, the thickness of film at SS = 162 was calculated from the weight loss as 8 μm assuming 100% porous film. The film thickness actually observed in the SEM cross-section was 15-20 μm. This means that the film was roughly 50% porous. The thickness at SS = 32 from weight loss was found to be 9.7 μm assuming 100% porous film. The film thickness observed in the SEM cross-section was 15-20 μm, meaning the film was about 60% porous.

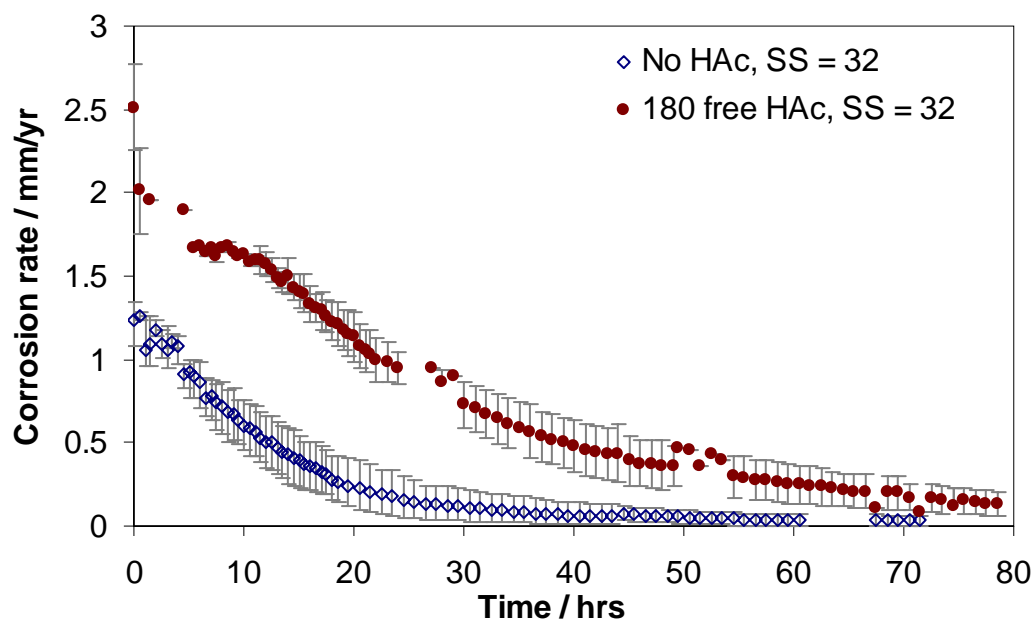


Figure 5.29: Average corrosion rate variation with time in experiments without and with 180 ppm free HAc (10000 ppm HAc total) at SS= 32, pH 6.6, 80°C, 10 ppm Fe²⁺ (Error bars represent the maximum and minimum values of corrosion rate observed, refer to Figure 5.30 for the curves in the logarithmic scale, 5.31 for SEM front view and 5.32 for SEM cross-sectional view.)

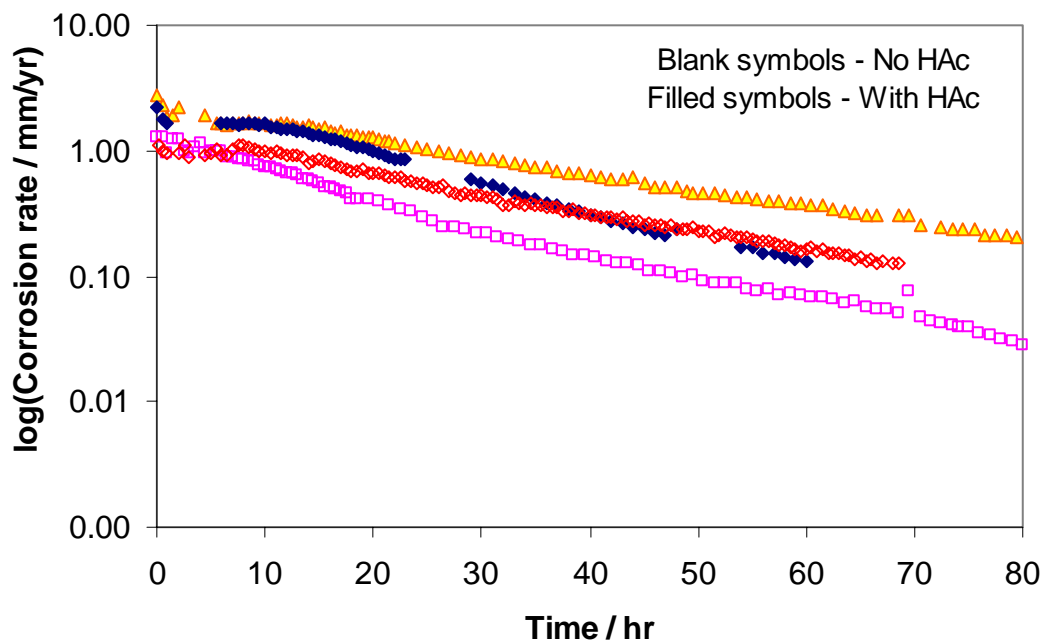
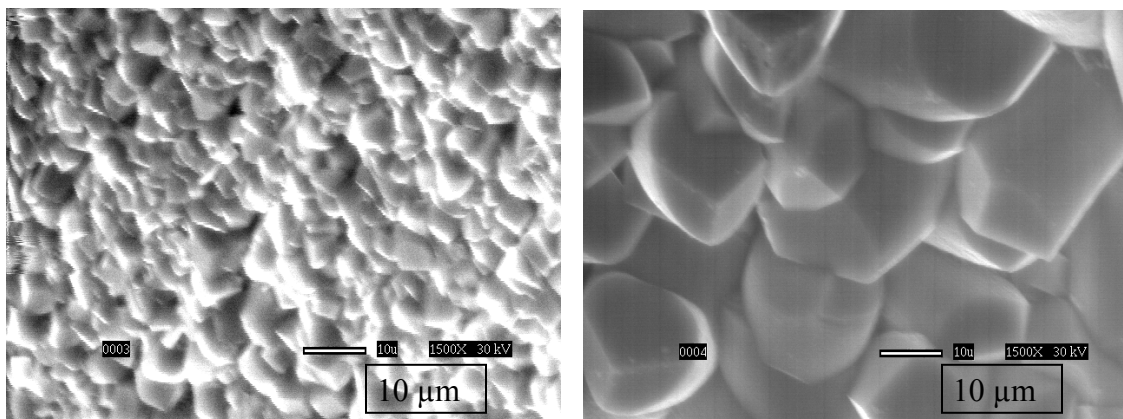


Figure 5.30: Corrosion rate progression with time in the logarithmic scale at SS = 32, pH 6.6, $T = 80^{\circ}\text{C}$, 10 ppm Fe^{2+} , without and with 180 ppm free HAc, stagnant conditions. (Refer to Figure 5.29 for the average curves, 5.31 for SEM front view and 5.32 for SEM cross-sectional view.)

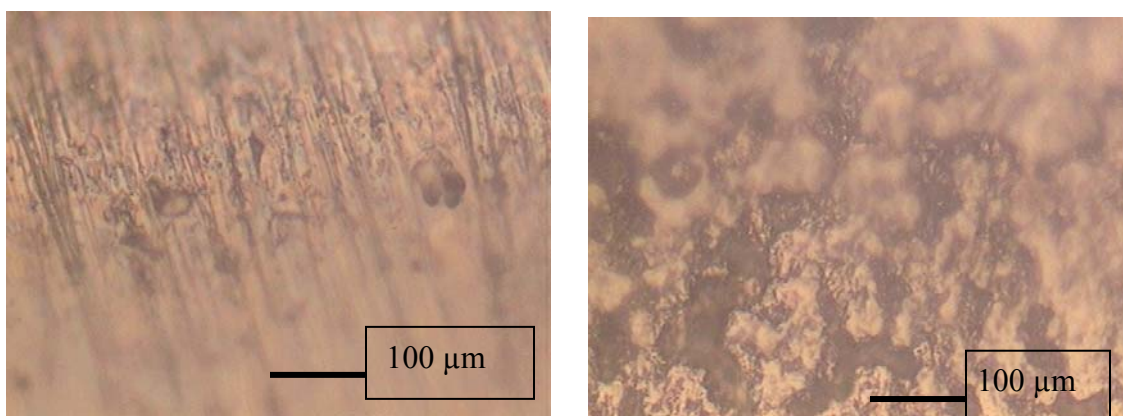
a) SEM pictures (frontal view) at 1500 X



Without HAC

With 180 ppm free HAC

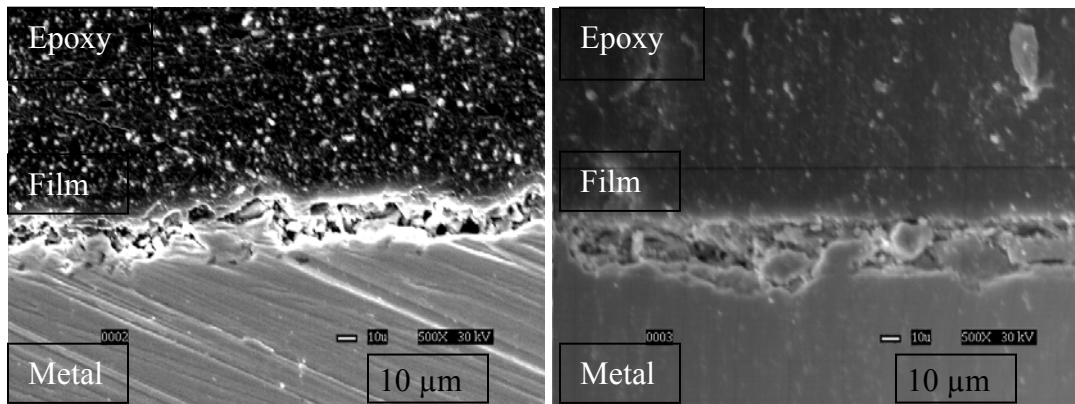
b) Optical microscope pictures at 600X



Film removed (without HAC)

Film removed (with 180 ppm free HAC)

Figure 5.31: Front view pictures of FeCO_3 film at SS = 32, pH 6.6, 80°C, 10 ppm Fe^{2+} , without and with 180 ppm free HAC, stagnant condition. (Refer to Figure 5.29 for the average curves, 5.30 for the curves in the logarithmic scale, 5.32 for SEM cross-sectional view)



Without HAC

With 180 ppm free HAC

Figure 5.32: SEM pictures (cross sectional view) of FeCO_3 film at 500 X, SS = 32, pH 6.6, 80°C, 10 ppm Fe^{2+} , 180 ppm free HAC, stagnant condition. (Refer to Figure 5.29 for the average curves, 5.30 for the curves in the logarithmic scale, 5.31 for SEM front view)

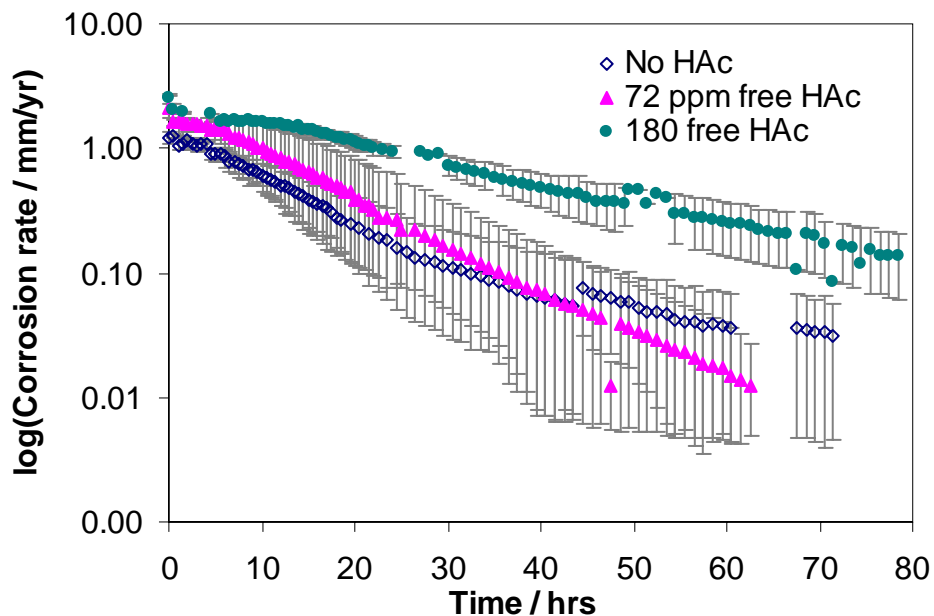


Figure 5.33: Comparison of the average curves at SS = 32, pH 6.6, 80°C, 10 ppm Fe^{2+} , with 72 and 180 ppm free HAC, stagnant condition in the logarithmic scale. (Error bars represent maximum and minimum values of corrosion rates)

5.5 Supersaturation (SS) of 10

Without and with 68 ppm free HAC:

Average corrosion rate variation with time was then studied at pH 6 (lowest supersaturation, even less favorable film forming conditions, maximum amount of free HAC) both without and with HAC. This is shown in Figure 5.34 The average curve without HAC and with 68 ppm free HAC each consists of four repeatable experiments. We observe that the corrosion rates starts at a higher value (about 2.5 mm/yr) and remains constant throughout the duration of the experiment. Figure 5.35 shows the corrosion rates of all experiments performed on a logarithmic scale. This shows that no protective film is formed at pH 6 even after 3 days, since corrosion rate does not drop. It is also confirmed

by the increase in the Fe^{2+} count taken after 24 hours showing that iron from the specimen is being added to the system through corrosion. It can be said that there is an equilibrium between film formation and corrosion.

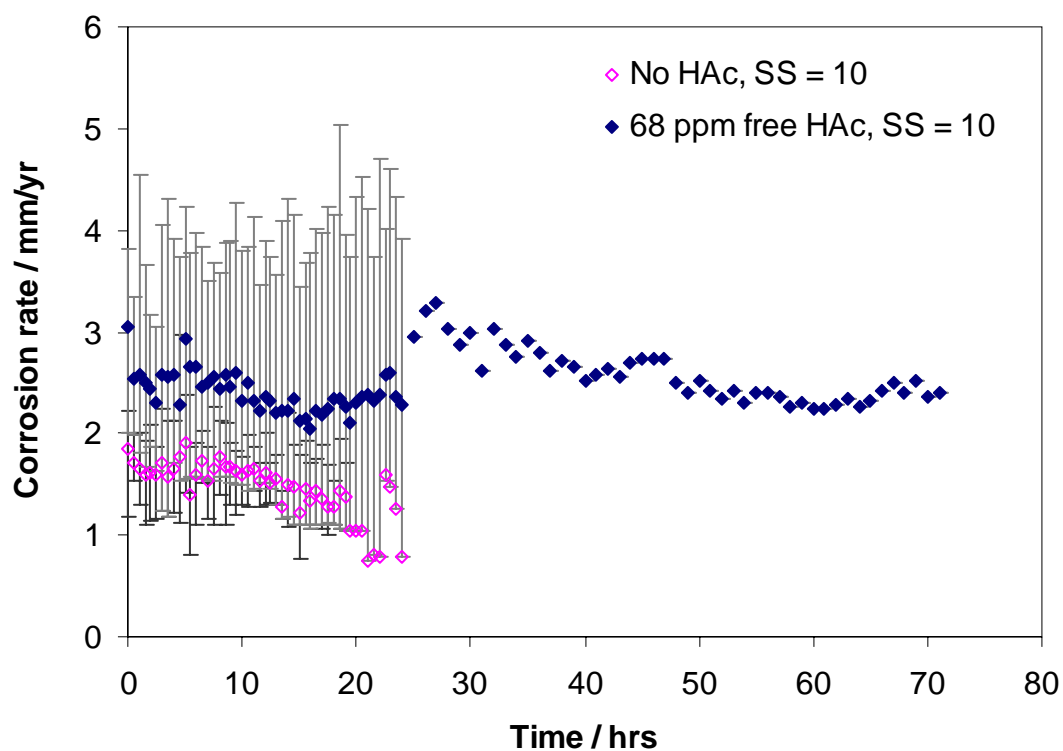


Figure 5.34: Average corrosion rate with time in experiments with and without 68 ppm free HAc (1000 ppm HAc total) at SS = 10, pH 6, 80°C, 50 ppm Fe^{2+} (Error bars represent the maximum and minimum values of corrosion rate observed, refer to Figure 5.35 for the curves in the logarithmic scale)

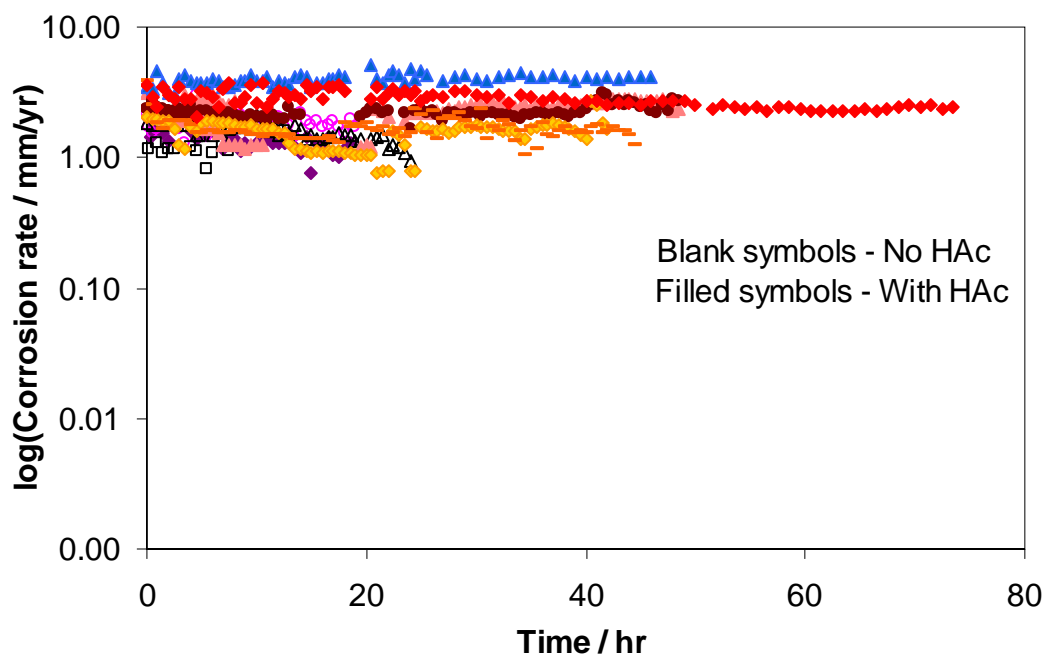


Figure 5.35: Corrosion rate progression with time in the logarithmic scale at SS = 10, pH 6, T = 80°C, 50 ppm Fe²⁺, without and with 68 ppm free HAc, stagnant conditions. (Refer to Figure 5.34 for the average curves.)

Last but not least, it was important to determine that the film observed is indeed FeCO₃. We can see from the Pourbaix diagram at the range of pH (6-6.6) and temperature (80°C) that FeCO₃ is the only thermodynamically stable species. In order to see the FeCO₃ spectrum and match it with the kind of film observed, an XRD scan was conducted as shown in Figure 5.36. We can see a good match with the theoretical FeCO₃ spectrum²⁴, confirming the presence of a FeCO₃ film. The extra peak observed at a Bragg's angle of 45° was found²⁴ to be of carbon.

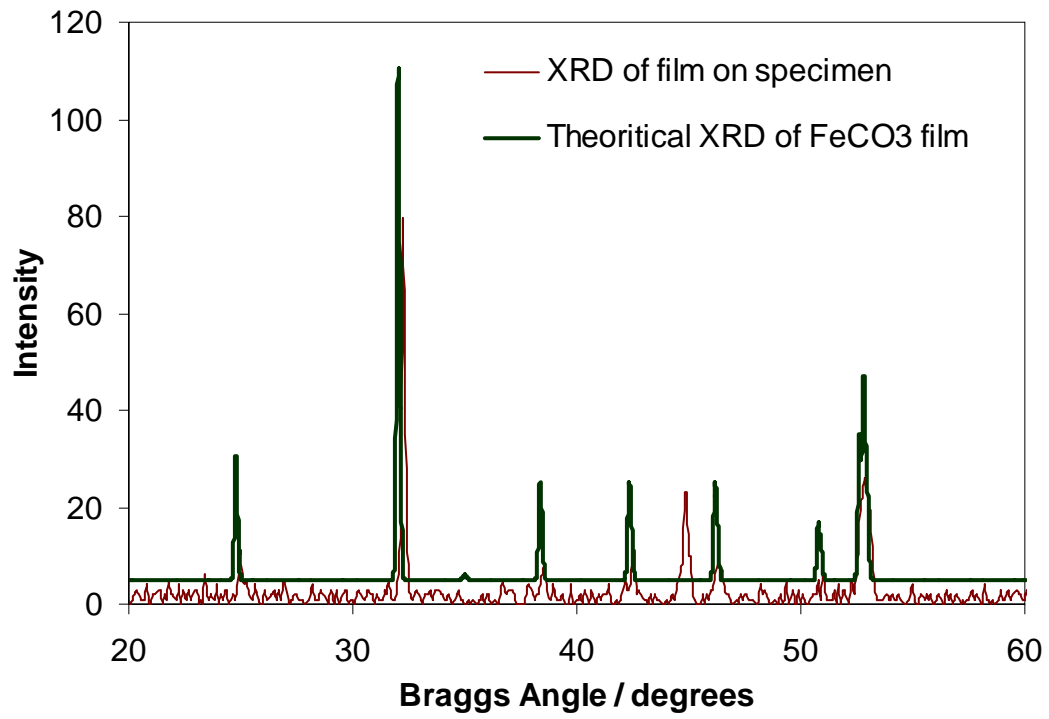


Figure 5.36: XRD Spectrum of protective film showing it to be iron carbonate.

5.6 Discussion

The rate of iron carbonate precipitation is dependent on the SS value which in turn is a function of Fe^{2+} concentration and pH as seen from Equation 2.17.

$$SS = f(Fe^{2+}, pH) \quad (2.17)$$

Thus at a fixed pH the amount of HAc added does not influence the SS and precipitation of iron carbonate film. It is seen from Equation 2.13 that the SS can be expressed as

$$SS = \frac{[Fe^{2+}][CO_3^{2-}]}{[K_{spFeCO_3}]} \quad (2.13)$$

K_{spFeCO_3} depends on temperature, which is constant, $[CO_3^{2-}]$ depends on pH, which is also fixed at some value, $[Fe^{2+}]$ is 50 ppm, so the SS value is fixed. Thus the amount of HAc added should have no effect on the protectiveness of films formed as long as the pH does not change. This is precisely what is observed in the experiments. The higher the pH the faster and more adherent a film is formed. Even though 1000 ppm of HAc (total) was added to the system, which is very high, we adjust the pH to the desired value by adding $NaHCO_3$.

The thickness of film formed is also not a true indication of the protectiveness offered. SEM cross-section view has shown that even though the thickness is of the order of 10 to 15 μm the film is very protective. This is also reflected in the corrosion rates determined by the LPR method. Another factor worth mentioning is the size of $FeCO_3$ crystals observed. It was found that in some cases, the presence of HAc resulted in an increase in the crystal size (refer to SEM front view pictures at 1500X in Figure 5.8a and

Figure 5.31a to that compared with experiments without HAc. This can be explained by the difference in nucleation rates. When the nucleation is uniform we have an even precipitation of protective film which yields lower crystal size. But if nucleation is non-uniform we can get bigger crystals on the same area since they have lateral space to grow. Again this difference in crystal size was found to have no effect on the film protectiveness.

5.7 Comparison with MULTICORP Version 3.0

The experimental results without and with HAc were compared with MULTICORP Version 3.0, the OU Corrosion prediction model²⁶. Corrosion rates obtained from the model and the experimentally observed average corrosion rates with and without HAc were plotted and compared. The OU model was also used to predict the thickness and porosity of the iron carbonate scale for different conditions and then compared with that obtained in experiments. Two cases were selected to compare with the model. These took into account the highest and lowest concentrations of free HAc tested (i.e. 18 and 180 ppm) and SS of 162 and 32 which represent the highest and second lowest values of supersaturations tested.

Case 1:

SS	Free HAc (ppm)	Fe ²⁺	pH
162	0	50	6.6
162	18	50	6.6

Case 2:

SS	Free HAc (ppm)	Fe ²⁺	pH
32	0	10	6.6
32	180	10	6.6

In both cases the simulation was run for 80 hours and compared with the average experimental values.

Case 1: Without and with 18 ppm free HAc at SS = 162, pH 6.6:

Figure 5.37 shows the comparison at SS=162, pH 6.6, 80°C, without and with 18 ppm free HAc, stagnant conditions. The starting corrosion rate with MULTICORP is higher than that experimentally observed for both without and with HAc, but it is reasonably accurate in predicting the final corrosion rates. The model predicts different starting corrosion rates for without and with HAc because the presence of HAc has an effect in increasing the corrosion rate⁹. Figure 5.38 shows the iron carbonate film thickness comparison at the same conditions and MULTICORP shows a thicker film (76.7 μm) than that actually obtained ($\sim 20 \mu\text{m}$). It shows a similar discrepancy in thickness in the experiment without HAc. The important thing is that although it over predicts the film thickness (not a reliable tool for corrosion rate prediction), it accurately predicts the final corrosion rate in presence of HAc.

Case 2: Without and with 180 ppm free HAc at SS = 32, pH 6.6:

Figure 5.39 shows the comparison at SS=32, pH 6.6, 80°C, without and with 180 ppm free HAc, stagnant conditions. Again the starting corrosion rate with MULTICORP is higher ($\sim 8 \text{ mm/yr}$) in the case of corrosion rate in the presence of 180 ppm free HAc than that experimentally observed. The model over predicts the corrosion rate with 180 ppm free HAc in the time interval of 0-10 hours but it is accurate in predicting the corrosion rates later and the final corrosion rates. The model needs to be tuned further in order to predict the initial corrosion rates more accurately. Figure 5.40 shows the representative

iron carbonate film thickness with 180 ppm free HAc compared to that experimentally observed. MULTICORP again shows a thicker film (38.4 μm) than that actually obtained ($\sim 25 \mu\text{m}$). In the case without HAc the discrepancy is similar which is expected since the SS value is unaffected by HAc addition as long as the pH is fixed.

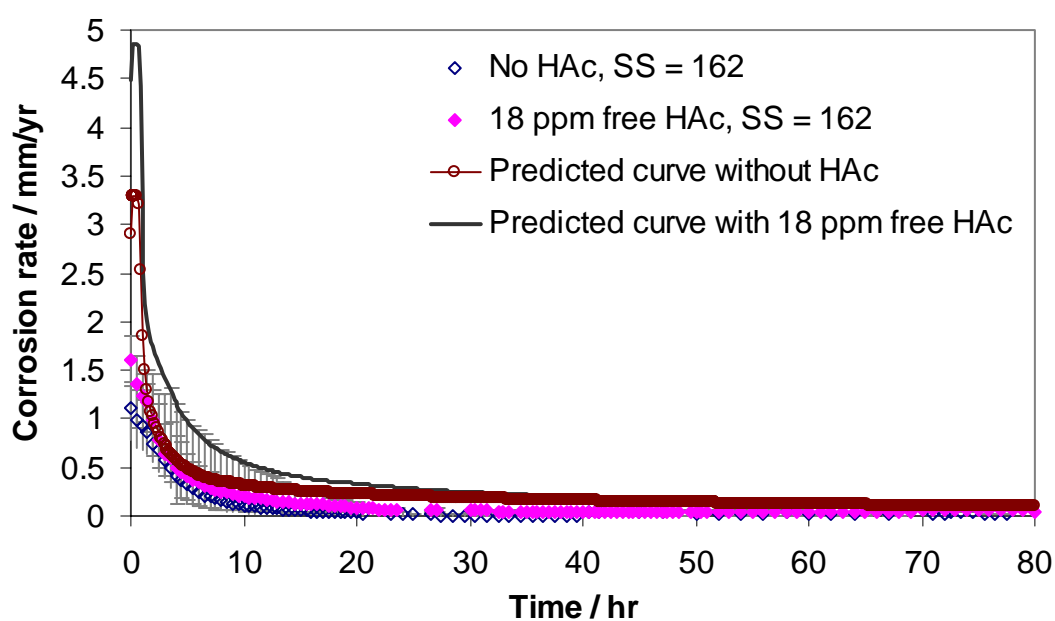


Figure 5.37: Comparison of experimental results with OU model at SS = 162, pH = 6.60, 80°C, 50 ppm Fe²⁺, without and with 18 ppm free HAc, stagnant conditions. (Data points indicate experimental results and lines indicate OU model, refer to Figure 5.38 for the comparison of film thicknesses.)

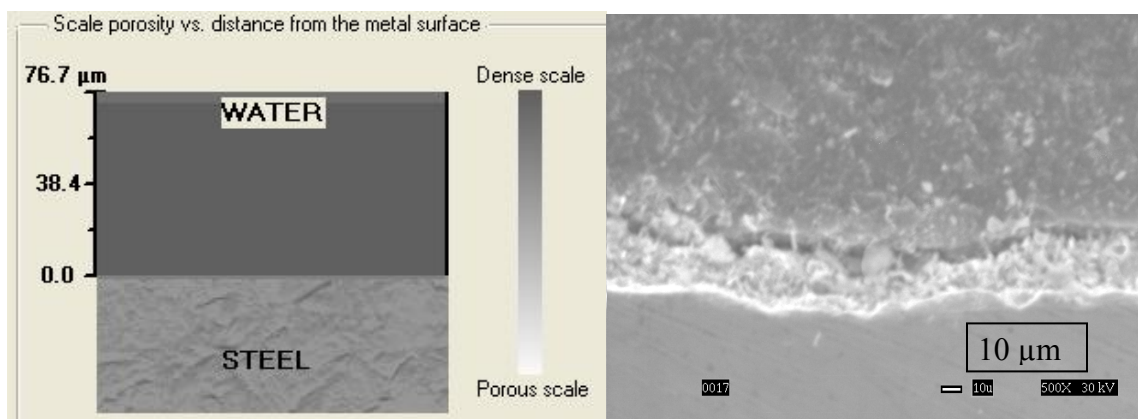


Figure 5.38: Predicted and experimentally measured iron carbonate scale thickness, at SS = 162, pH = 6.60, 80°C, 50 ppm Fe²⁺ with 18 ppm free HAc, stagnant conditions. (Refer to Figure 5.37 for the corrosion rate comparison.)

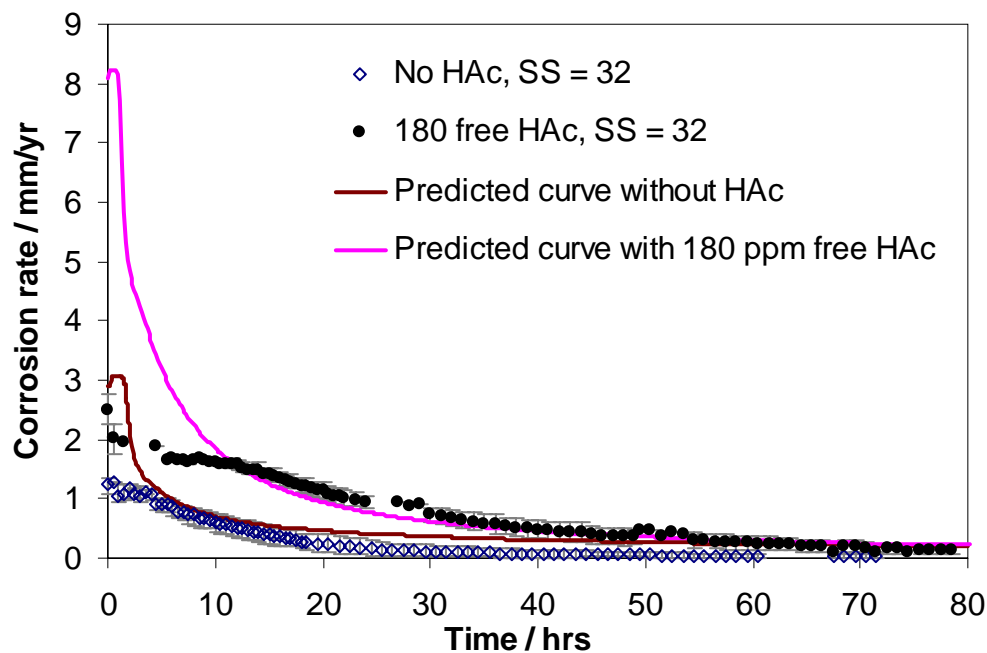


Figure 5.39: Comparison of experimental results with OU model at SS = 32, pH = 6.60, 80°C, 10 ppm Fe²⁺ without and with 180 ppm free HAc, stagnant conditions. (Data points indicate experimental results and lines indicate OU model, refer to Figure 5.40 for the comparison of film thicknesses.)

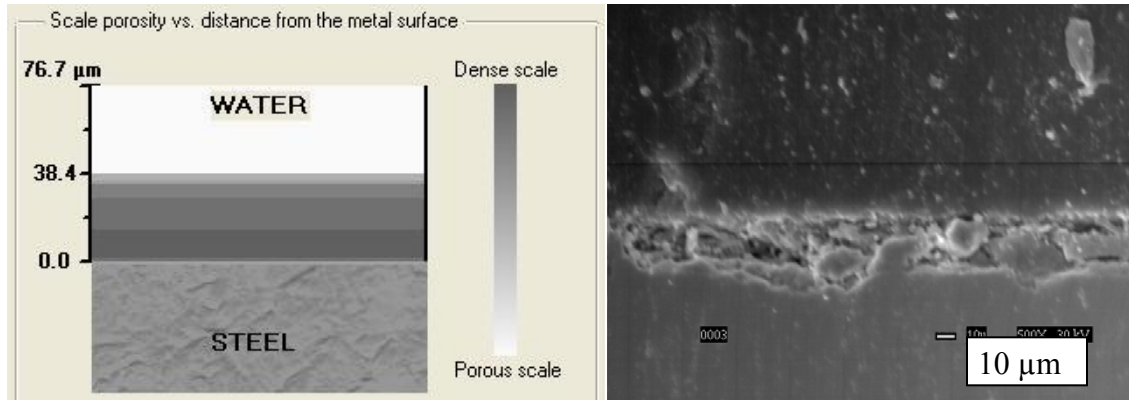


Figure 5.40: Predicted and experimentally measured iron carbonate scale thickness, at SS = 32, pH = 6.60, 80°C, 10 ppm Fe²⁺ with 180 ppm free HAc, stagnant conditions. (Refer to Figure 5.39 for the corrosion rate comparison.)

Finally, a comparison of the porosity of the film obtained by weight loss method at SS = 162, and SS = 32 without HAc was done with the MULTICORP model.

At SS = 162, a 50% porous film of thickness 15 to 20 μm was observed experimentally without HAc. The average film porosity obtained from the model under the same conditions was 56%. At SS = 32, a 60% porous film of thickness 15 to 20 μm was observed experimentally without HAc. The average film porosity obtained from the model under the same conditions was 57%.

Thus in both cases tested we get a good match with the actual porosity of the film.

6. Conclusion

The effect of free HAc on iron carbonate film formation and protectiveness has been studied in a glass cell, RCE assembly at four different SS values of 162, 41, 32 and 10. Experiments included those at pH 6.6, 6.3 and 6 at stagnant conditions with and without HAc and those at 9000 rpm at SS of 162 in the presence of 72 ppm free HAc. The free HAc concentrations tested include 18, 35, 68, 72 and 180 ppm. All experiments were done at a constant pH and at a temperature of 80°C.

Based on this work, the important findings which emerge both from the experiments and MULTICORP comparison are:

- There is no effect of free HAc on iron carbonate film formation and protectiveness at a fixed pH. Iron carbonate film structure and crystal size are more or less unaffected by the presence of HAc. No effect of rotational velocity is observed on the film integrity in the presence of 72 ppm free HAc at SS of 162, pH 6.6.
- There is no evidence of localized corrosion, and no instance of iron acetate complex formation was observed.
- MULTICORP over predicted the initial corrosion rate as well as the film thickness at the two cases tested. The final corrosion rates are in good agreement with those experimentally observed, although further tuning of the model is required.

References

1. C. deWaard, D.E. Milliams, "Carbonic Acid Corrosion of Steel", *Corrosion* Volume 31, No.5, 1975, p 175.
2. S. Nestic, J. Postlethwaite, S. Olsen, "An Electrochemical Model For Prediction of CO₂ Corrosion", CORROSION/1995, Paper No. 131, (Houston, TX: NACE International, 1995)
3. S. Nestic, M. Nordsveen, R. Nyborg, A. Stangeland, "A Mechanistic Model for CO₂ Corrosion with Protective Iron Carbonate Films", CORROSION/2001, Paper No. 1040, (Houston, TX: NACE International, 2001)
4. S. Nestic, M. Nordsveen, R. Nyborg, A. Stangeland, "A Mechanistic Model for CO₂ Corrosion with Protective Iron Carbonate Films-Part 1: Theory and Verification", *Corrosion*, Volume 59, No.5, 2003, p 443-456.
5. A. Dugstad, "The Importance of FeCO₃ Super-saturation on CO₂ Corrosion of Carbon Steels" CORROSION/1992, Paper No.14, (Houston, TX: NACE International, 1992)
6. J.L. Crolet, M.Bonis, "The Role of Acetate Ions in CO₂ Corrosion", CORROSION/1983, Paper No. 160, (Anaheim, CA: NACE International, 1983)
7. B. Hedges, L.McVeigh, "The Role of Acetate in CO₂ Corrosion: The Double Whammy", CORROSION/1999, Paper No. 21, (Houston, TX: NACE International, 1999)
8. Y.K. Kharaka, "Solmineq 88: A Computer Program for Geochemical Modeling of Water-Rock Interactions", Alberta Research Council, Menlo Park, CA, 1989.

9. K. George, "Electrochemical Investigation of CO₂ Corrosion of Mild steel in the Presence of Acetic acid", Master of Science Thesis, Ohio University, March 2003.
10. D. Sidorin, "The Influence of Acetate on the Corrosion of Steel in CO₂ Saturated Brines", Master of Philosophy Thesis, September 2003, University of Southampton, U.K
11. J.L. Crolet, N. Thevenot, and A. Dugstad., "Role of Free Acetic acid on the CO₂ Corrosion of Steels", CORROSION/1999, Paper No. 24, (Houston, TX: NACE International, 1999)
12. Y. Garsany, D. Pletcher, B. Hedges., "The Role of Acetate in CO₂ Corrosion of carbon steel: Has the Chemistry been forgotten?", CORROSION/2002, Paper No. 02273, (Houston, TX: NACE International, 2002)
13. Y. Garsany, D. Pletcher, B. Hedges, "The Role of Acetate in CO₂ Corrosion of Carbon Steel: Studies Related to Oilfield Conditions" CORROSION/2003, Paper No. 03324, (Houston, TX: NACE International, 2003)
14. Y. Garsany, D. Pletcher, B. Hedges., "Speciation and Electrochemistry of Brines Containing Acetate Ion and Carbon dioxide", *J Electroanalytical Chemistry*, 538-539, 2002, p 285-297.
15. M. Joosten, J. Kolts. J.W. Hembree, M. Achour, "Organic acid Corrosion in Oil and Gas Production" CORROSION/2002, Paper No. 02273, (Denver, CO: NACE International, 2002)
16. M.L. Johnson, M.B. Thomson, "Ferrous Carbonate precipitation kinetics and its impact on CO₂ Corrosion", CORROSION/1991, Paper No. 268, (Cincinnati, OH: NACE International, 1991)

17. Van Hunnick E.W.J., B.F.M. Pots and E.L.J.A.Hendriksen, "The Formation of Protective FeCO₃ Corrosion Product Layers in CO₂ Corrosion" CORROSION/1996, Paper No. 6, (Houston, TX: NACE International, 1996)
18. A. Ikeda, M.Ueda, S. Mukai, "CO₂ Behavior of Carbon and Cr Steels", Advances in CO₂ Corrosion- Ed. R.H. Hausler. (Houston, TX, NACE International, 1984)
19. Videm, A. Dugstad, "Corrosion of Carbon Steel in Aqueous CO₂ environment", *Materials Performance*, March 1989, p 63-67.
20. G. Schmitt, M. Mueller, M. Papenfuss, E. Stobel-Effertz, "Localized CO₂ Corrosion of Carbon Steel from Physical Properties of Iron Carbonate Scales", CORROSION/1999, Paper No. 38, (Houston, TX: NACE International, 1999)
21. M.Stern, "A Method for Determining Corrosion Rates from Linear Polarisation Data", *Corrosion*, Volume 14, p 440, 1959.
22. G.S. Haynes and R. Baboian, Ed, *Laboratory Corrosion Tests and Standards*, ASTM Special Publication 866, 1983, p 505-509.
23. D.A.Jones, *Principles and Prevention of Corrosion*, 2nd edition, ISBN 0-13-359993-0, 1996.
24. International Center for Diffraction Data (ICDD) Database, Powder Diffraction File (Inorganic phases, alphabetic index) 1989.
25. J.M. Bockris, D. Drazic. A.R. Despic, *Electrochemica Acta*, Volume 4, p 325, 1961.
26. S. Nesic, S.Wang, J. Cai, Y. Xiao, "Integrated CO₂ Corrosion- Multiphase Flow Model", CORROSION/2004, Paper No. 04626. (Houston, TX: NACE International, 2004)

APPENDIX A: METHOD OF Fe²⁺ ADDITION

1. Deionised water (DI water) (100mL) was deoxygenated in a small beaker for about 10-15 minutes.
2. 1.78 g FeCl₂.4H₂O was weighed in a weighing dish.
3. FeCl₂ was added into the deoxygenated DI water.
4. After FeCl₂ was dissolved, the required amount of solution was removed out of the glass cell using a syringe and was added to the test solution by piercing the needle through the septum on the glass cell.
5. The amount of iron chloride solution added to the test solution to achieve a required concentration of Fe²⁺ (ppm), when 1.78 gm of FeCl₂.4H₂O is dissolved in 100 ml deoxygenated solution is given by the equation:

$$V = \frac{[Fe^{2+}] * V_{Total} * 100}{\left(\frac{W}{MW}\right)_{FeCl_2.4H_2O}} \quad (A-1)$$

where,

V is the volume needed to be added in the test (ml), V_{Total} is the total volume of the test solution, in liters (2 l), W is the weight of FeCl₂.4H₂O added (1.78 gm), MW is the molecular weight of FeCl₂.4H₂O. (198 gm)

Simplifying the above, we get

$$V(ml) = \frac{Fe^{2+}(ppm)}{MW_{Fe^{2+}} * 1000} * \frac{V_{Total}(l) * 100(ml)}{\left(\frac{W}{MW}\right)_{FeCl_2.4H_2O}} \quad (A-2)$$

Substituting the known values, we get

$$V(ml) = \frac{Fe^{2+}}{56 * 1000} * \frac{2 * 100}{\left(\frac{1.78}{198}\right)_{FeCl_2 \cdot 4H_2O}} \quad (A-3)$$

Hence, from the above equation, if a concentration of 50 ppm of Fe^{2+} , is needed, a 20 ml of the prepared $FeCl_2 \cdot 4H_2O$ solution is needed.

6. $FeCl_2 \cdot 4H_2O$ solution was always added before the metal sample was inserted in the solution.

APPENDIX B: TAFEL SLOPES

Stern²¹ (1959) described β_a and β_c as the slopes of the logarithmic local anodic and cathodic polarisation curves respectively. β_a , β_c can be expressed as a function of temperature:

$$\beta_a = \frac{2.303RT}{\alpha_a F} \quad (\text{B-1})$$

$$\beta_c = \frac{2.303RT}{\alpha_c F} \quad (\text{B-2})$$

where,

T is absolute temperature in K, R is the universal gas constant (8.314 J/mol K), and α_a and α_c are the symmetry factors for anodic and cathodic reaction. The values of α_a and α_c are 1.5 and 0.5 as explained by the Bockris mechanism²⁵. F is Faraday's constant (96,496 coulombs/equivalent).

From the above equations the 'B' value can be calculated using the following expression:

$$B = \frac{\beta_a \beta_c}{2.303(\beta_a + \beta_c)} \quad (\text{B-3})$$

From equations B-1, B-2 and B-3 the average 'B' value was calculated to be 14.5 mV/dec.

After the formation of an iron carbonate film, the cathodic reaction might become diffusion- controlled. Hence, under those conditions the cathodic Tafel slope (β_c) could be assumed to become infinite. This is not strictly speaking correct but is a reasonable

approximation. By substituting the value of β_c as infinity in equation (B-3) and evaluating the 'B' value, it was calculated to be 19.44 mV. In the actual experimental conditions, there would be film-formation as well as non film-formation conditions. An average of the above two B values was taken when calculating the corrosion rates by LPR method without HAc. Thus the B value used was given as

$B = (14.5+19.44)/2 = 17 \text{ mV/dec}$. This value was used for all experiments without HAc.

The β_a and β_c values used in all experiments with HAc were obtained from George⁹ (2003) from the potentiodynamic sweeps. At 80°C, he obtained $\beta_a = 95 \text{ mV/dec}$ and $\beta_c = 140 \text{ mV/dec}$ giving a 'B' value of 24 mV/dec. This value was taken for calculating the corrosion rates in the presence of HAc.

APPENDIX C: CORROSION RATE MEASUREMENT

The corrosion rate was monitored using the linear polarization resistance (LPR) technique. From basic electrochemical theory, the corrosion current density i_{corr} can be described as:

$$i_{corr} = B * \frac{1}{R_p} * \frac{1}{A} \quad (C-1)$$

where,

B is the 'B' value as explained in Appendix B, Equation B-3, R_p is the polarization resistance in ohm, A is the electrode area in m^2 .

The corrosion rate (CR) in mm/yr can then be calculated²³ according to the following equation:

$$CR = \frac{m}{At\rho} = \frac{i_{corr}M_w}{\rho nF} = 1.16 * i_{corr} \quad (C-2)$$

where,

m is the metal loss in kg, A is the electrode surface area in m^2 , t is the time in seconds, ρ is the density of the iron (7870 kg/m^3), i_{corr} is the current density in A/m^2 , "M_w" is the atomic weight of iron in grams, F is the Faraday constant and n is the number of electrons exchanged in the electrochemical reaction.

APPENDIX D: EXPERIMENTAL UNCERTAINTY ANALYSIS

D.1 Uncertainty in the corrosion rate measurement due to instrumentation.

The factors that affect the accuracy of the LPR corrosion rate measurements include temperature, applied current, applied potential and the working electrode area.

According to Appendix C, the corrosion rate can be written as,

$$CR = 1.16 * i_{corr} \quad (D-1)$$

where CR is expressed in mm/yr, and i_{corr} is in A/m^2 .

From equations 4.1, B-3 and D-1,

$$CR = 0.503 \frac{\beta_a \beta_c}{(\beta_a + \beta_c)} \times \frac{1}{R_p} \quad (D-2)$$

Since, β_a and β_c depend only on temperature and vary linearly with temperature as seen from Equation B-1 and B-2. They can be rewritten as follows:

$$\beta_a = \beta_{a0} + m_1 T \quad (D-3)$$

$$\beta_c = \beta_{c0} + m_2 T \quad (D-4)$$

where, β_{a0} and β_{c0} are the base anodic and cathodic Tafel constant at a suitable reference temperature (25°C). Slopes m_1 and m_2 can be easily obtained by plotting Equation B-1 and B-2. The values obtained are $m_1 = 0.015$ mV/K and $m_2 = -0.045$ mV/K.

In equation (D-2), R_p can be expressed as follows:

$$R_p = \frac{dE}{di_{app}} \quad (D-5)$$

where, i_{app} is the applied current density in A/m^2

$$i_{app} = \frac{I_{app}}{a} \quad (D-6)$$

where, I_{app} is the applied current in A and a is the working area in cm^2

Substituting equation (D-3) into (D-6) in equation (D-2), we get

$$CR = 0.503 \frac{(\beta_{a0} + m_1 T)(\beta_{c0} + m_2 T)}{\beta_{a0} + \beta_{c0} + (m_1 + m_2)T} \times \frac{\Delta I_{app}}{\Delta E \Delta a} \quad (D-7)$$

The above equation can then be written in the following form:

$$CR = 0.503 * (\beta_{a0} + m_1 T)(\beta_{c0} + m_2 T)[\beta_{a0} + \beta_{c0} + (m_1 + m_2)T](\Delta I_{app})(\Delta E)^{-1}(\Delta a)^{-1} \quad (D-8)$$

The sensitivity of small changes in the corrosion rate to small changes in each variable is expressed by taking partial derivatives of the corrosion rate with respect to each variable. The errors in β_{a0} , β_{c0} , m_1 and m_2 are assumed to be negligible. Thus, the absolute uncertainty in the measurement of corrosion rate because of uncertainties in the system variables can be expressed as follows:

$$\frac{\delta(CR)}{CR} = \left[\frac{\partial(CR)}{\partial T} \right] \frac{\delta T}{CR} + 2 \left[\frac{\partial(CR)}{\partial E} \right] \frac{\delta E}{CR} + 2 \left[\frac{\partial(CR)}{\partial I_{app}} \right] \frac{\delta I_{app}}{CR} + 2 \left[\frac{\partial(CR)}{\partial a} \right] \frac{\delta a}{CR} \quad (D-9)$$

Deriving the partial derivatives of each item above according to equation (D-8) and then substituting into (D-9), the following equation is obtained:

$$\frac{\delta(CR)}{CR} = \left(\frac{m_1}{\beta_a} + \frac{m_2}{\beta_c} \right) \delta T - \frac{2}{E} \delta E + \frac{2}{I_{app}} \delta I_{app} - \frac{2}{a} \delta a \quad (D-10)$$

Therefore, the corrosion rate uncertainty above can be considered an overall uncertainty through the experiment for the LPR technique. It considers the uncertainties due to the temperature, due to instrumentation (potential and applied current), and

working electrode surface area. The contribution of each item in (D-10) to the corrosion rate uncertainty measurements is calculated as follows:

Temperature

The temperature during the experiment was maintained at $80^{\circ}\text{C} \pm 1^{\circ}\text{C}$, thus $\delta T=1$. Tafel slopes calculated at 80°C are, $\beta_a = 46 \text{ mV}$ and $\beta_c = 140 \text{ mV}$. Hence the first part on the right hand side of the equation (D-10) is:

$$\left(\frac{m_1}{\beta_a} + \frac{m_2}{\beta_c} \right) \delta T = \left(\frac{0.015}{46} + \frac{-0.045}{140} \right) \times 1 = 4.658 * 10^{-6} \quad (\text{D-11})$$

Potential

According to Gamry, the DC accuracy in voltage measurement is $\pm 0.3\%$, $\pm 1 \text{ mV}$. During the experiment, the applied potential was $\pm 5 \text{ mV}$ over the open circuit potential. Thus the uncertainty in the potential would be $\delta E = 1.03 \text{ mV}$. The error in the potential could be different for measurements before and after formation of the iron carbonate scale or the inhibitor film. Before the formation of the scale, the R_p was determined over the entire applied potential since there was a linear relationship between the potential and the current, as shown in Figure D.1. Hence, the absolute uncertainty due to the potential in equation (D-10) can be described as:

$$\frac{2}{E} \delta E = \frac{2}{10} \times 1.03 = 0.206 \quad (\text{D-12})$$

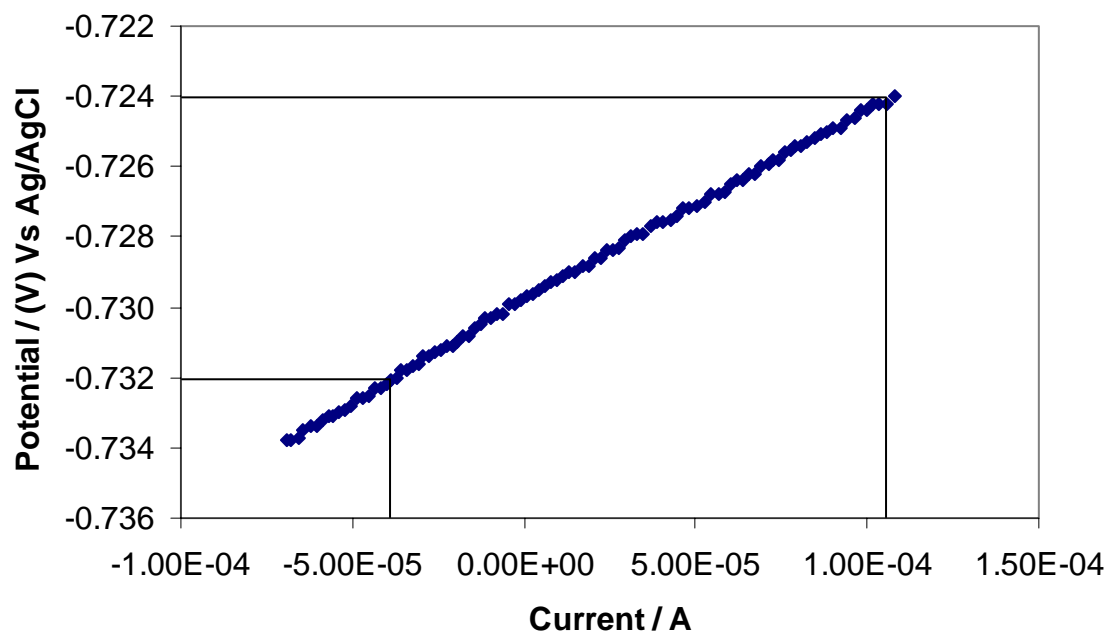


Figure D.1: A typical linear polarization curve obtained in experiments before film formation.

However, after the film was formed on the metal surface, the linear relationship did not exist over the entire applied potential, as indicated in Figure D.2. The actual potential used to get the R_p was only taken from the linear region, which was a 6 mV range. Thus the absolute uncertainty after the scale formation is:

$$\frac{2}{E} \delta E = \frac{2}{6} \times 1.03 = 0.343 \quad (\text{D-13})$$

Hence, depending on when the LPR was taken, the error due to the potential measurement should be somewhere between with and without scale formation

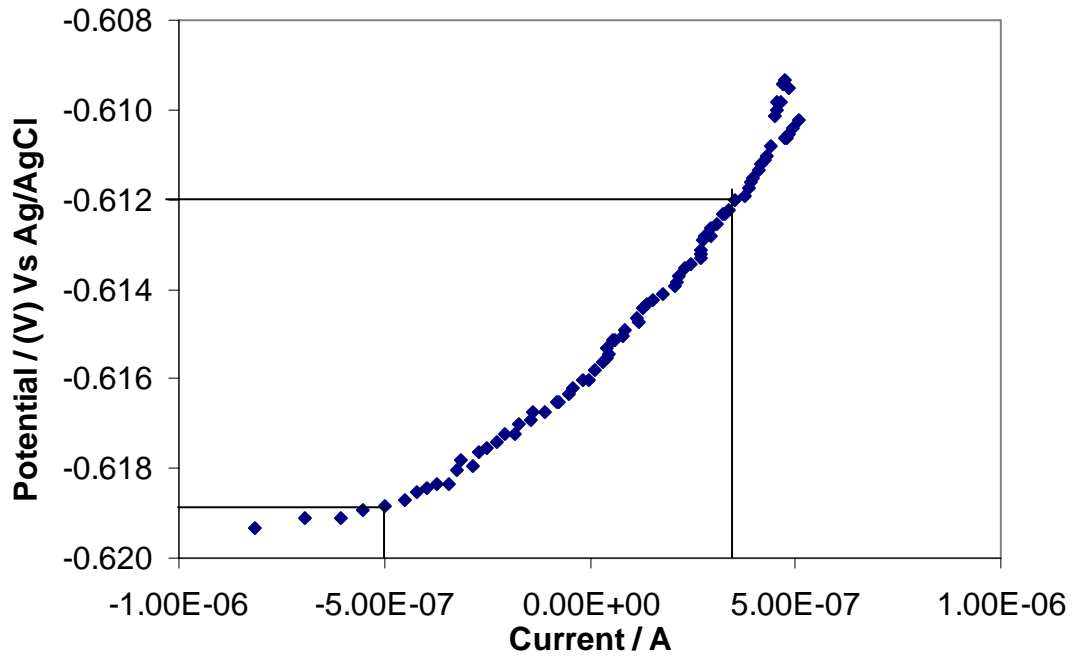


Figure D.2: A typical linear polarization curve obtained in experiments after film formation.

Current

According to Gamry, the DC accuracy in current measurement is $\pm 0.3\%$, ± 50 pA. The current range was different for different experiments, and varied with time because of the change in the corrosion rate. At the start of the experiment, the applied current range is usually around $400 \mu\text{A}$. Thus the uncertainty in the current would be:

$$\delta I_{app} = 4 \times 10^{-4} \times 0.003 = 1.2 \times 10^{-6} \text{ A} \quad (\text{D-14})$$

Hence, the absolute uncertainty in the equation (D-10), due to the current would be:

$$\frac{2}{I_{app}} \delta I_{app} = \frac{2}{4 \times 10^{-4}} \times 1.2 \times 10^{-6} = 6.0 \times 10^{-3} \quad (\text{D-15})$$

After the formation of the film, since the corrosion rate is reduced, the applied current was reduced to about 4 μA . Thus the uncertainty in the current would be:

$$\delta I_{app} = 1.2 \times 10^{-8} \text{ A} \quad (\text{D-16})$$

Hence, the absolute uncertainty in the equation (D-10) due to the current would be

$$\frac{2}{I_{app}} \delta I_{app} = \frac{2}{4 \times 10^{-6}} \times 1.2 \times 10^{-8} = 6.0 \times 10^{-3} \quad (\text{D-17})$$

Electrode Area

The uncertainty in the area is due to the accuracy of the measuring instrument, the loss of area due to the polishing of the sample and corrosion loss of the reused sample. It was estimated to be 0.01 cm^2 . Therefore, the absolute uncertainty due to the surface area in equation (D-10) is:

$$\frac{2}{a} \delta a = \frac{2}{5.4} \times 0.01 = 3.7 \times 10^{-3} \quad (\text{D-18})$$

Thus the uncertainties in the corrosion rate measurement from the LPR technique for the specified experiment are expressed as:

$$\frac{\delta(CR)}{CR} = \pm \left(4.658 \times 10^{-6} - \frac{0.206 + 0.343}{2} + 6.0 \times 10^{-3} - 3.7 \times 10^{-3} \right) = \pm 27.68\% \quad (\text{D-19})$$

From the above equations, it can be concluded that in the LPR measurement technique, the uncertainty in the potential is a major source of error in the corrosion rate. The error calculated in equation (D-18) would be the average error over entire length of the experiment. Hence, at the beginning of the experiment, the error could be about 20% while, towards the end of the experiment, after formation of the iron carbonate scale or the inhibitor film the error could be 34%.

D.2 Uncertainty in the corrosion rate measurement due to initial conditions

Error in the initial conditions, such as pH and Fe^{2+} concentrations could have an effect on the precipitation rate of iron carbonate. Since corrosion is affected by the precipitation of the scale, this could lead to uncertainty in the corrosion rate.

The uncertainty in the added Fe^{2+} concentration is due to the error associated with the syringe. The syringe used to inject Fe^{2+} has an accuracy of ± 0.1 ml. Since the least amount of Fe^{2+} used for an experiment was 10 ml, the absolute error due to Fe^{2+} is given by:

$$\frac{\delta Fe}{Fe} = \frac{0.1}{10} = 0.01 \quad (D-20)$$

The pH meter has an accuracy of ± 0.01 pH units. At a pH of 6.60, a change in the pH by ± 0.01 units could cause a change in the CO_3^{2-} ion concentration by ± 0.0004 M.

Since at pH 6.60, the CO_3^{2-} ion concentration is 0.0178 M, the absolute error due to the pH meter is given by:

$$\frac{\delta CO_3^{2-}}{CO_3^{2-}} = \frac{0.0004}{0.0178} = 0.022 \quad (D-21)$$

The error caused in the measurement of the pH meter (CO_3^{2-} ion concentration) and the Fe^{2+} concentration, leads to uncertainty in the supersaturation (SS). Supersaturation is related to Fe^{2+} concentration and CO_3^{2-} ion concentration by equation (2.12). If the error in solubility product due to the temperature is negligible, the uncertainty in the supersaturation can be found out from the following equation:

$$\frac{\delta(SS)}{SS} = \frac{\delta Fe}{Fe} + \frac{\delta CO_3^{2-}}{CO_3^{2-}} = 0.01 + 0.022 = 0.032 \quad (D-22)$$

The supersaturation was varied from 10-162. Hence, the errors at different supersaturations are as follows:

$$\text{At SS} = 10, \delta(\text{SS}) = 0.032 * 10 = 0.32$$

$$\text{At SS} = 32, \delta(\text{SS}) = 0.032 * 32 = 1.024$$

$$\text{At SS} = 41, \delta(\text{SS}) = 0.032 * 41 = 1.321$$

$$\text{At SS} = 162, \delta(\text{SS}) = 0.032 * 162 = 5.184$$

This error in the supersaturation could affect the precipitation rate that in turn affects the corrosion rate. However, there is no explicit equation showing the relation between precipitation rate and the corrosion rates. Due to this implicit error, the uncertainty in the corrosion rates for the precipitation experiments could be more than that calculated from the Appendix D.1.

D.3 Comparison of the experimental and the calculated error

The absolute error of the experiments without HAc at SS = 162 and SS = 32 as shown in the average curves in Figure 5.3 and Figure 5.26 is calculated and compared to the error calculated in Appendix E.1. The comparison is shown in Figure D.3 and Figure D.4. The experimental error was found by taking the average of maximum and minimum of the corrosion rate and then dividing it by the average corrosion rate in the experiment. From the plots, it is seen that the experimental error is much lower than the calculated error of 27.68 %.

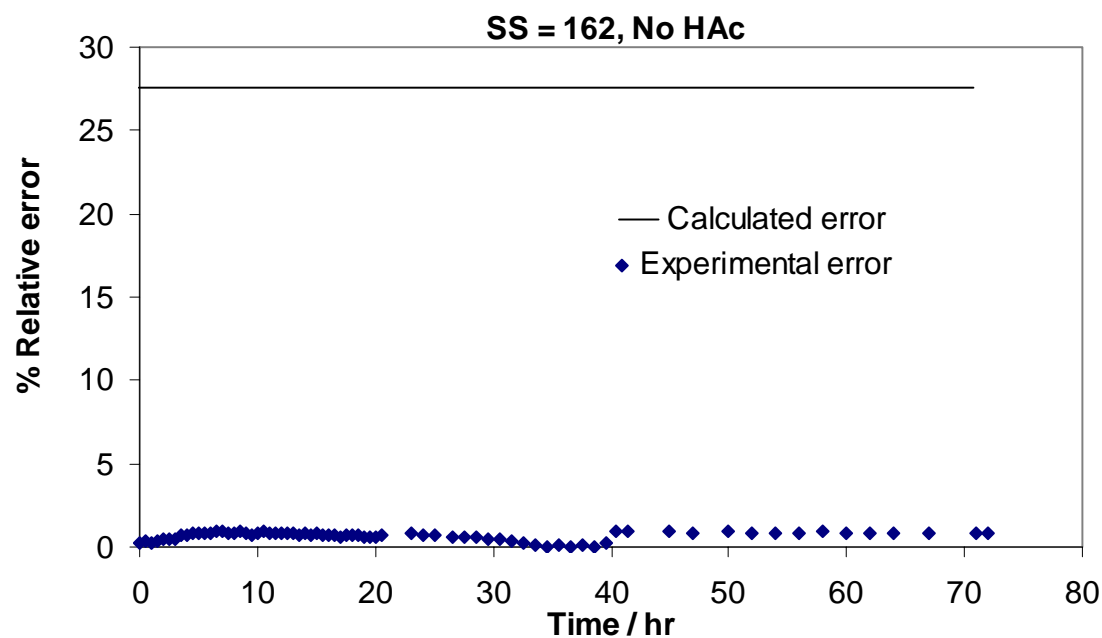


Figure D.3: Comparison of the calculated and the experimental error at supersaturation of 162 and $T = 80^{\circ}\text{C}$.

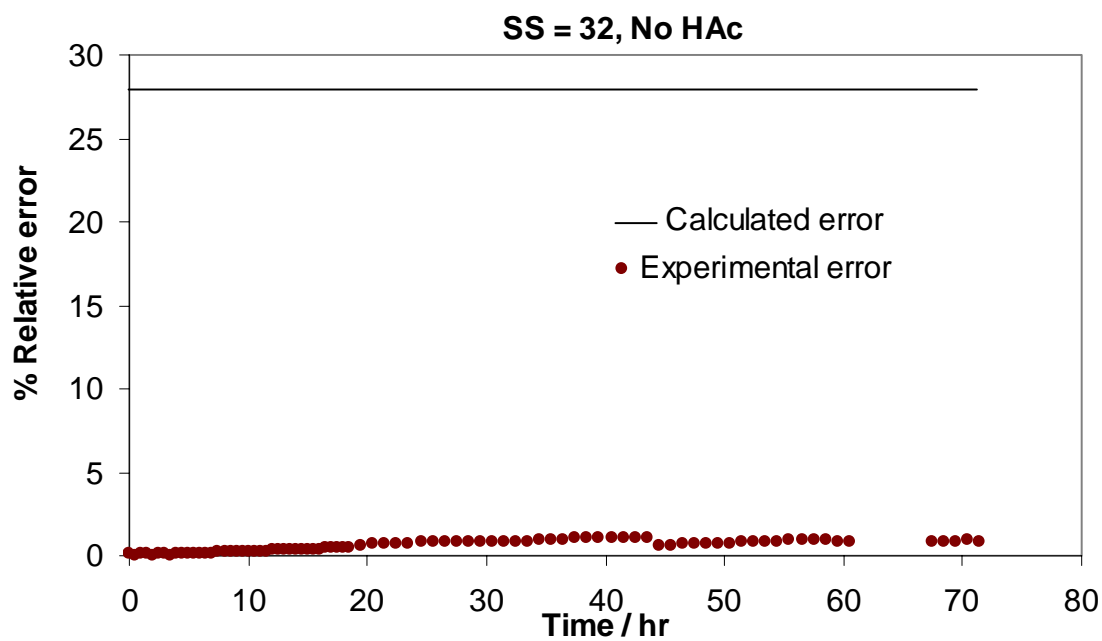


Figure D.4: Comparison of the calculated and the experimental error at supersaturation of 32 and $T = 80^{\circ}\text{C}$.

APPENDIX E: SUPERSATURATION CALCULATION

The supersaturation (SS) value at a certain pH and Fe^{2+} concentration was calculated from Equation 2.13:

$$SS = \frac{[Fe^{2+}][CO_3^{2-}]}{[Ksp_{FeCO_3}]}$$

Thus at 80°C, pH 6.6, the $[CO_3^{2-}] = 2.78 \cdot 10^{-5}$ mol/l. Taking into account the ionic strength of the solution, the $Ksp_{FeCO_3} = 1.54 \cdot 10^{-10}$. $[Fe^{2+}]$ is either 50 or 10 ppm.

Thus at 80°C, pH 6.6, 50 ppm Fe^{2+} ($8.95 \cdot 10^{-4}$ mol/l),

$$SS = (8.95 \cdot 10^{-4}) * (2.78 \cdot 10^{-5}) / (1.54 \cdot 10^{-10}) = 162$$

At 80°C, pH 6.6, 10 ppm Fe^{2+} ($1.79 \cdot 10^{-4}$ mol/l),

$$SS = (1.79 \cdot 10^{-4}) * (2.78 \cdot 10^{-5}) / (1.54 \cdot 10^{-10}) = 32$$

At 80°C, pH 6.3, 50 ppm Fe^{2+} ($8.95 \cdot 10^{-4}$ mol/l), $[CO_3^{2-}] = 6.99 \cdot 10^{-6}$ mol/l

$$SS = (8.95 \cdot 10^{-4}) * (6.99 \cdot 10^{-6}) / (1.54 \cdot 10^{-10}) = 41$$

At 80°C, pH 6, 50 ppm Fe^{2+} ($8.95 \cdot 10^{-4}$ mol/l), $[CO_3^{2-}] = 1.76 \cdot 10^{-6}$ mol/l

$$SS = (8.95 \cdot 10^{-4}) * (1.76 \cdot 10^{-6}) / (1.54 \cdot 10^{-10}) = 10$$

APPENDIX F: METHOD OF SAMPLE CLEANING USING CLARKE'S SOLUTION

The composition of Clarke's solution is as shown below:

Parameter	Amount
Hydrochloric acid (HCl, sp gr. 1.19)	1 litre
Antimony trioxide (Sb ₂ O ₃)	20 g
Stannous chloride (SnCl ₂)	50 g
Temperature	room
Time	up to 25 min.

1. The Clarke's solution should be vigorously stirred and the specimen should be rubbed with a non-abrasive implement made of wood or rubber.
2. After dipping in Clarke's solution for 10 seconds, the sample was removed and a rubber eraser was used to remove the film in the weight loss experiments as well as while taking the optical microscope pictures.
3. After rubbing the sample weight was recorded and the procedure repeated until the bare metal was visible. This entire process took about an hour of vigorous rubbing suggesting that the film was indeed very hard to remove.
4. The possibility for removal of solid metal is present which results in error in the determination of the corrosion rate. To prevent this, the cleaning procedure is repeated and weighed after each cleaning, the ordinate at the intersection of the

mass loss and corrosion product weight loss curves is the mass loss caused by the removal of corrosion products alone.(Reference #22, p 510)